NASA SP-8085

NASA SPACE VEHICLE DESIGN CRITERIA (ENVIRONMENT)

THE PLANET MERCURY (1971)

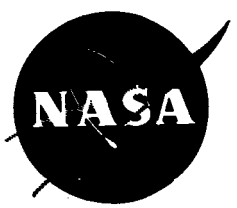

MARCH 1972

NATIONAL AERONAUTICS AND SPACE ADMINISTRATION

FOREWORD

NASA experience has indicated a need for uniform criteria for the design of space vehicles. Accordingly, criteria are being developed in the following areas of technology:

Environment
Structures
Guidance and Control
Chemical Propulsion

Individual components of this work will be issued as separate monographs as soon as they are completed. A list of the monographs published in this series can be found on the last page.

These monographs are to be regarded as guides to design and not as NASA requirements except as may be specified in formal project specifications. It is expected, however, that the monographs will be used to develop requirements for specific projects and be cited as the applicable documents in mission studies and in contracts for the design and development of space vehicle systems.

This monograph was prepared under the cognizance of the Goddard Space Flight Center with Scott A. Mills as program coordinator. The principal author was Neil Divine of the Jet Propulsion Laboratory. Valuable contributions were also made by A. J. Beck, F. D. Palluconi, and R. A. Schiffer of the Jet Propulsion Laboratory.

Comments concerning the technical content of these monographs will be welcomed by the National Aeronautics and Space Administration, Goddard Space Flight Center, Systems Reliability Directorate, Greenbelt, Maryland 20771.

March 1972

For sale by the National Technical Information Service, Springfield, Virginia 22151 — Price $3.00

CONTENTS

1. INTRODUCTION 1

2. STATE OF THE ART 1

2.1 Physical Properties 1
- 2.1.1 Mass
- 2.1.2 Dimensions and Mean Density
- 2.1.3 Orbit and Rotation

2.2 Gravity Field 3

2.3 Magnetic Field and Magnetosphere 4

2.4 Electromagnetic Radiation 4
- 2.4.1 Solar Radiation
- 2.4.2 Mercury Reflected Radiation
- 2.4.3 Mercury Thermal Emission
- 2.4.4 Mercury Microwave Emission
- 2.4.5 Other Radiation Sources

2.5 Charged Particles 9
- 2.5.1 Galactic Cosmic Rays
- 2.5.2 Solar Particle Events
- 2.5.3 Solar Wind

2.6 Atmosphere 10
- 2.6.1 Pressure
- 2.6.2 Temperature
- 2.6.3 Composition
- 2.6.4 Models

2.7 Surface 14
- 2.7.1 Features
- 2.7.2 Physical Conditions
  - 2.7.2.1 Surface Composition
  - 2.7.2.2 Soil Mechanical Properties
  - 2.7.2.3 Topography
- 2.7.3 Electromagnetic Properties
- 2.7.4 Temperature and Thermal Properties

3. CRITERIA 21

3.1 Physical Properties 21

3.2 Gravity Field 21

3.3 Magnetic Field and Magnetosphere 21

3.4 Electromagnetic Radiation 25

3.5 Charged Particles 26
3.6 Atmosphere 26
3.7 Surface 29
REFERENCES 42
APPENDIX A. DEFINITIONS OF SYMBOLS 49
APPENDIX B. ATMOSPHERIC STRUCTURE RELATIONS 53
APPENDIX C. GLOSSARY 55
NASA SPACE VEHICLE DESIGN CRITERIA MONOGRAPHS 59

THE PLANET MERCURY (1971)

1. INTRODUCTION

The design of space vehicles intended to encounter and investigate the planet Mercury requires both quantitative and qualitative descriptions of Mercury's environment. The information presented in this monograph is based on 1970 state-of-the-art. At this time original, quantitative data published for Mercury are so limited that they can be almost fully summarized by the entries in the four tables I, II, III, and V except for mass, radius, magnitude, color, and orbital data, and observations of diffuse features on Mercury's disk. The data are supplemented by a considerable variety of published theoretical analyses.

During the search for and acquisition of Mercury information for evaluation and inclusion in this monograph, assessments were made of the potential effects of environmental properties on vehicle performance so that descriptions appropriate for vehicle and subsystem design could be formulated. In particular the electromagnetic radiation field must be described thoroughly in terms of light to permit efficient design of optical and solar cell power supply systems, and in terms of heat for thermal control systems. Solar protons and solar wind fluxes, far more severe near Mercury than near the Earth, may damage or introduce unwanted signals in subsystems containing electronic devices. If there is an atmosphere surrounding Mercury, its composition, temperature, and density influence the design of aeroshells and heat shields. Lastly, surface rock and soil temperatures, and mechanical properties are required if lander support and locomotion systems are to be designed.

Because these design criteria are not specific to a particular mission, they are set without reference to the circumstances of Mercury encounter. For this reason the ranges of the parameters cited include the effects of variability and inhomogeneity, where applicable, as well as of observational uncertainty.

References 1, 2 and 3 describe electromagnetic, magnetic field, and meteoroid environments which apply both in transit to and near Mercury. Pertinent symbol definitions, mathematical formulations, and a glossary are contained in appendices A, B, and C respectively.

2. STATE OF THE ART

2.1 Physical Properties

The physical properties considered here are the planetary mass, dimensions, mean density, and motions of orbit and rotation. Photometric and physical properties of the surface are discussed in sections 2.4 and 2.7.

2.1.1 Mass

The mass M_M of Mercury is determined from analysis of its gravitational effect on the positions and orbits of planets, asteroids, and spacecraft in the inner solar system. The positions are derived from optical observations of planets and asteroids, radar observations of planets, and radio signal observations of spacecraft. The analysis often includes the determination of other quantities (in addition to Mercury's mass) in a consistent way, particularly planetary orbital elements, radii, and masses. Klepczynski et al. (ref. 4) review several independent determinations, and present the final weighted mean $M_\odot/M_M = 5\,987\,000 \pm 32\,000$ for the ratio of the mass of the Sun to the mass of Mercury. Because this mean is based on a comprehensive survey of available results and because its uncertainty overlaps those of various, thorough modern determinations (refs. 5, 6 and 7), it is adopted here. Taking $M_\odot = (1.989 \pm 0.002) \times 10^{33}$ g (ref. 8), the value $M_M = (3.32 \pm 0.02) \times 10^{26}$ g results for the mass of Mercury.

2.1.2 Dimensions and Mean Density

The radius R_M of Mercury has been measured by standard optical techniques, by photometric observations during transit (passage between Earth and Sun), and by radar reflection measurements. Of major review articles (refs. 9 and 10), the latest by Dollfus (ref 10) specifies $R_M = 2432 \pm 7$ km. Melbourne et al. (ref. 6) adopt $R_M = 2435 \pm 3$ km, primarily on the basis of radar measurements which are intrinsically the most precise (ref. 5). The error quoted in reference 6 (±3 km) is much smaller than the lunar relief which is of the order of ±6 km (ref. 11).

This relief masks the likely overall deformation of Mercury from a sphere, of the order of a few meters (ref. 12), or, for the moon, of about 1 km (ref. 8). There are no direct measures of Mercury's deviation from a sphere, and the published literature cites zero values for Mercury's oblateness (ref. 8). Thus, this monograph adopts a radius $R_M = 2435 \pm 6$ km encompassing nominal and extreme distances of the solid surface from Mercury's center. The corresponding mean density is $\bar{\rho} = 3M_M/4\pi R_M^3 = 5.5 \pm 0.1$ g/cm^3.

2.1.3 Orbit and Rotation

Details of Mercury's orbital motion are provided by the *American Ephemeris and Nautical Almanac* (ref. 13).* Some of its orbital parameters are shown in table VIII (sec. 3.1). Mercury's orbital ellipticity and inclination to the ecliptic are greater than that of any other known planet except Pluto. It is the nearest known planet to the Sun.

Telescopic observations of the indistinct features on Mercury's surface (sec. 2.7.1) formed the basis for widespread opinion prior to 1965 that Mercury's rotational angular velocity ω_r equals its mean orbital angular velocity n so that the same hemisphere faces the Sun at all times, as the moon faces the Earth. The corresponding sidereal rotation period T_r equals the orbital period $T_o = 87.969$ days (ref. 8). The analysis of radar signals reflected from Mercury has invalidated this opinion and has implied instead prograde rotation with a

*For a precise ephemeris, see "Development Ephemeris 69" in JPL TR32-1465.

sidereal period of 59 ±5 days (ref. 14). Reanalysis of the telescopic data has narrowed the range of rotation periods to 58.67 ±0.03 days (ref. 15), 58.625 ±0.03 days (ref. 16), or 58.663 ±0.021 days (ref. 17).

These results are all consistent with the resonance* relationship $T_r = (2/3)T_o = 58.646$ days. Theoretical discussions have shown that this resonance can be stable (refs. 18 and 19). Thus, this monograph adopts the value $T_r = 58.646 \pm 0.03$ days, including the uncertainty of the telescopic observations which has been applied to the resonance period. The corresponding rotational angular velocity is $\omega_r = 2\pi/T_r = (1.2400 \pm 0.0006) \times 10^{-6}$ rad/sec, nearly equal to the orbital angular velocity $n(1-e)^{-2}$ at perihelion passage. This near equality implies a stable rotation rate and suggests that near Mercury's perihelion the Sun moves very slowly in the sky as seen from Mercury's surface and provides intense radiation for several weeks at some longitudes.

The prime meridian (longitude zero) of the Hermocentric longitude system is that adopted by the International Astronomical Union, contains the subsolar point at the perihelion passage about 10 January 1950, and assumes prograde rotation with the resonance period $T_r = (2/3)T_o$. Figures 1 and 2 (sec. 3.1) show the nature of the resonance in heliocentric and Hermocentric longitude, respectively. At Mercury's equator, longitudes 0° and 180° are subsolar points near alternate perihelion passages and are called "hot poles" (ref. 20). Similarly, equatorial longitudes 90° and 270° are subsolar points near alternate aphelion passages and are called "warm poles", because they receive less solar energy per "day" on Mercury (176 terrestrial days) than the "hot poles".

Observations of surface features (sec. 2.7.1) and radar data (sec. 2.7.3) have set approximate upper bounds on the inclination of Mercury's rotational equator to its orbital plane. The upper limit adopted here for this inclination is 10° (ref. 21) and includes the estimates cited in the literature. The actual inclination is probably much smaller.

2.2 Gravity Field

The uncertainty in Mercury's mass (sec. 2.1) is so large that the harmonic and centrifugal terms which are appropriate for some other planets may be excluded. Thus, the gravitational potential may be expressed as

$$\Psi = -\frac{GM_M}{R} \quad . \tag{1}$$

This potential leads to expressions for the surface acceleration of gravity $g = GM_M/R^2_M$, the escape velocity $V_e = (2GM_M/R)^{1/2}$, and the period of circular orbit about Mercury $T_a = 2\pi a^{3/2}/(GM_M)^{1/2}$. The following quantities, evaluated from the mass M_M and radius R_M adopted in sec. 2.1, are required for the entries in table IX (sec. 3.2):

*See Glossary, appendix C.

$$GM_M/R_M = (9.10 \pm 0.07)\ km^2/sec^2 \quad (2)$$

$$g = GM_M/R_M{}^2 = 374 \pm 4\ cm/sec^2 \quad (3)$$

$$(2GM_M/R_M)^{1/2} = (4.27 \pm 0.02)\ km/sec \quad (4)$$

$$\text{and } 2\pi R_M{}^{3/2}/(GM_M)^{1/2} = 5072 \pm 35\ sec = 84.5 \pm 0.6\ min. \quad (5)$$

The mass concentrations (mascons) suggested for Mercury (on the basis of lunar analogy and the spin-orbit resonance) by O'Leary et al. (ref. 22) have effects on the foregoing quantities smaller than the uncertainties resulting from uncertainties in Mercury's mass and radius. Therefore, mascon effects are ignored herein.

2.3 Magnetic Field and Magnetosphere

There are no data that directly indicate existence of an intrinsic magnetic field of Mercury. Three apparently independent estimates of the surface field strength are of the order of 10^{-2} gauss (refs. 23, 24 and 25). Reiffel (ref. 26) assumes no intrinsic magnetic field for Mercury because of its slow rotation. (Fast rotation is thought to be significant in the maintenance of the fields of the Earth and Jupiter.) The range of magnetic moments corresponding to the foregoing estimates is between zero and the upper limit $M_1 = 4 \times 10^{23}$ gauss-cm^3. The corresponding magnetic field strengths range from the lower limit of 10γ, a low interplanetary field estimate near Mercury (ref. 27), to $2M_1/R^3$ where $2M_1/R_M{}^3 = 2800\gamma$.

The boundary of the magnetosphere is fixed by the interaction of the planetary field with the solar wind (sec. 2.5.3). For the minimum field estimates the magnetosphere is nonexistent, but the maximum field estimates yield a magnetosphere boundary one planetary radius above the surface in the solar direction and slightly larger elsewhere. If a magnetosphere exists, its configuration is probably similar to the Earth's (ref. 2) except that the distortions caused by the Earth's rotation should be neglected. In these circumstances the simple expression adapted from Good (ref. 25) can be expected to describe the shape of the magnetosphere's outer boundary as follows:

$$R = R_1\ (4 - \cos\theta)/3. \quad (6)$$

Here R_1 is the sunward extent (for Mercury $R_1 < 2R_M$) and θ is the angle from the solar direction.

2.4 Electromagnetic Radiation

The electromagnetic radiation environment near Mercury includes the X-ray, ultraviolet, visible, infrared, and microwave portions of the spectrum.

2.4.1 Solar Radiation

The solar radiation environment at one AU from the Sun is given in reference 1 which specifies the spectral irradiance P_λ (the received power per unit area and per unit wavelength interval) for all wavelengths between 1 Å and 100 cm. At the extremes of this range, i.e., the X-ray and microwave regions, the radiation is sporadic; but between 0.1 and 10 μm the radiation is steady with an integrated flux of S = 0.1353 ±0.0021 watt/cm^2 at one AU from the Sun, i.e., the solar constant (ref. 28). These quantities, S and P_λ, multiplied by r^{-2} (where r is the distance of Mercury from the Sun in AU) provide estimates of the radiation at Mercury. Because of the high eccentricity of Mercury's orbit (table VIII, sec. 3.1), r^{-2} ranges between 4.6 and 10.6 and, accordingly, the integrated flux S/r^2 ranges between 0.623 and 1.435 watt/cm^2 in the sunlight.

2.4.2 Mercury Reflected Radiation

Solar radiation reflected from Mercury has been measured visually and photographically by various observers whose results are discussed by Harris (ref. 29). The photoelectric measurements of Irvine et al. (ref. 30) are generally in agreement with the foregoing results at the few phase angles for which data are published, and are intrinsically more precise. Therefore, they are adopted here.

Mercury's astronomical magnitudes, m, phase function, $\phi(a)$, and geometric albedo, p (λ), whose definitions are given in appendix C and also in references 8 and 29, are satisfactorily approximated by the following expressions:

$$m = m_\odot - 2.5 \log [p(\lambda)\phi(a)] + 5 \log (rR/R_M) \tag{7}$$

$$\log \phi(a) = \frac{a}{250}\left[3.8 + \frac{a}{100}\left(-2.73 + \frac{a}{50}\right)\right] \tag{8}$$

$$\log p(\lambda) = (-0.94 \pm 0.07) + (0.25 \pm 0.05)(2-\lambda^{-1}). \tag{9}$$

These expressions have been adapted from Allen (ref. 8), Harris (ref. 29), and Irvine (ref. 30). The quantities are defined in appendix A; and the distance r from the Sun must be expressed in AU, the phase angle a in degrees, and the wavelength λ in μm. The apparent magnitude $m_\odot$ of the Sun is given at several wavelengths in table XII (sec. 3.4; ref. 29). Further details of photometric studies are in references 31, 32, and 33.

The flux of reflected sunlight may be calculated directly from the foregoing values of the phase function, $\phi(a)$, and the geometric albedo, $p(\lambda)$ by the formula

$$F_\lambda = \frac{p(\lambda)\phi(a)}{r^2(R/R_M)^2} P_\lambda \ . \tag{10}$$

Here, P_λ is the solar spectral irradiance specified in reference 1 and the distance r from the Sun must be expressed in AU. If the solid angle of the visible, sunlit portion of Mercury's

disk is Ω_M (which can be calculated from the applicable geometry with the values given in sec. 2.1), the intensity of the surface has the average value

$$I_\lambda = F_\lambda/\Omega_M. \quad (11)$$

The reflection properties of different portions of the disk imply that an uncertainty factor of 2 in either direction should be applied to the intensity (eq. 11) on the basis of lunar analogy (ref. 34). The uncertainties specified for the albedo (eq. 9) are large enough so that the uncertainties from substitution of the albedo values into expressions for magnitude and flux (eqs. 7 and 10) bracket the variations and uncertainties for all wavelengths and phase angles.

The polarization of the light reflected from Mercury varies with phase and position on the disk. The latest measurements reported by Dollfus (ref. 35) conclude that the polarization is similar to the moon's (ref. 36).

Although photometric observations of Mercury are not complete enough to permit a determination of the integrated or radiometric albedo (ref. 9), the similarity of the observed parameters to those of the moon suggests the adoption of lunar values for Mercury. For the moon, the range from 0.07 to 0.24 includes extremes based on differing surface terrains, and the average value is 0.12 (ref. 37).

2.4.3 Mercury Thermal Emission

The observational data from which the characteristics of Mercury's thermal emission have been inferred are discussed in section 2.7.4 and summarized in table V. In the wavelength range between 1 μm and 0.1 cm, thermal emission occurs within 100 wavelengths of the surface, and is therefore characteristic of the surface temperature and material properties (sec. 2.7). Although direct measurements of infrared emissivity are not available, it has been estimated as close to unity (ref. 21) and that value is adopted here. With the infrared emissivity taken as unity, the intensity and flux of thermal radiation are distributed in wavelength according to the Planck function $B_\lambda(T)$, which describes blackbody radiation, and the formulas in table XI (sec. 3.4) where T is the local surface temperature. That temperature is given in section 2.7.4, and various sources, e.g., Allen (ref. 8), tabulate the Planck function. The integrated flux incident on a spacecraft can be obtained only by integrating the intensities over wavelength and solid angle, but limiting values may be obtained in the form of σT^4 (the integral of the Planck function, ref. 8) where the limiting values of T are taken as 90° and 700°K (sec. 2.7.4). These temperature limits imply limits on the integrated flux of 0.0004 and 1.4 watt/cm^2 at Mercury's surface. At larger separations from Mercury ($R > R_M$), the flux limits are proportional to $(R/R_M)^{-2}$.

2.4.4 Mercury Microwave Emission

At wavelengths between 0.33 and 11.3 cm, Mercury's radio emission has been detected by several observers, including those listed in table I. The observational data have been inter-

*See Glossary, appendix C.

preted in terms of effective brightness temperature T_B which is related to the observed flux F_ν by the modified Rayleigh-Jeans formula,

$$F_\nu = 2\pi k T_B (R_M / r\lambda)^2 \quad . \tag{12}$$

Here the quantities involved are defined in appendices A and C. The brightness temperatures exhibit variations with wavelength and time of observation which exceed observational uncertainties and permit derivation of numerical values for physical, thermal, and electrical properties of Mercury's epilith or soil near the surface (sec. 2.7). The mean brightness temperatures, i.e., those averaged over a long interval of observation, derived at various wavelengths are shown in table I (adapted from ref. 38).

At some wavelengths the data reported in the references cited in table I are complete enough to indicate strong dependence of the brightness temperature on phase angle and its weaker dependence on heliocentric longitude. Because of the resonance* between the periods of Mercury's orbit and rotation (sec. 2.1.3), these dependences can be expressed in terms of the hermographic latitude, longitude, and the local time of that point on Mercury's surface directly beneath a nearby spacecraft.

These considerations are not pertinent to spacecraft design when the encounter circumstances are unspecified, but they do lead to a broad range of possible brightness temperatures at each wavelength. The range adopted here for design purposes is shown as a function of wavelength in figure 3 (sec. 3.4). The adopted values are based on the references given in table I. The tabulation of brightness temperatures vs wavelengths in table I indicates a probable increase of mean brightness temperature with wavelength between a few millimeters and several centimeters (ref. 38).

If the brightness temperature T_B is substituted for the physical temperature T in the formulas for the thermal emission given in section 2.4.3, the same formulas describe the microwave emission in the wavelengths from 0.1 to 20 cm.

2.4.5 Other Radiation Sources

Harris (ref. 29) describes the light reflected from the moon and planets visible from Mercury. The magnitudes of these objects varies with relative positions (including phase angle) and orientations (including rotation and Saturn's ring inclination) which are specified in the *American Ephemeris and Nautical Almanac* (ref. 13) or Woolley (ref. 47). Uncertainty broad enough to include these variations is implied by the expression for the apparent magnitude

$$m = (m_o \pm 0.3) + 5\, log\ (r\Delta) + (0.03 \pm 0.02)a \quad . \tag{13}$$

Appropriate definitions are given in appendix A, and table XII (sec. 3.4) specifies values of m_o for the several objects at several wavelengths obtained from reference 29. Magnitudes and colors of bright stars may be obtained from standard star catalogs.

*See Glossary, appendix C.

TABLE I

SUMMARY OF MERCURY'S RADIO BRIGHTNESS TEMPERATURE MEASUREMENTS

Wavelength (cm)	Mean Brightness Temperature, T_B* (°K)	Reference
0.33	296 ± 30	Epstein et al. (ref. 39)
0.34	277 ± 30	Epstein et al. (ref. 40)
0.80	530 ± 50	Golovkov & Losovsky (ref. 41)
1.53	450 ± 60	Welch et al. (ref. 42)
1.95	288 ± 30	Kaftan-Kassim & Kellermann (ref. 43)
1.95	350 ± 30	Morrison & Klein (ref. 38)
2.82	375 ± 40**	Morrison & Klein (ref. 38)
3.45, 3.75	400 ± 80	Howard et al. (ref. 44)
3.75	380 ± 20	Klein (ref. 45)
6.00	385 ± 20	Morrison & Klein (ref. 38)
11.3	300 ± 40	Kellermann (ref. 46)

*Uncertainty estimates by Morrison & Klein (ref. 38) rather than original authors in most cases.

**Unpublished results of Medd, cited by Morrison & Klein (ref. 38).

The integrated flux from the stars and planets is approximately $\sigma T^4 = 4.6 \times 10^{-10}$ watt/cm^2 where T = 3°K, the equivalent blackbody temperature of space (ref. 8). This flux is an appropriate lower limit for all spacecraft surfaces when shadowed from both the Sun and Mercury if Mercury is the nearest planet.

2.5 Charged Particles

Mercury's probable lack of magnetic field and atmosphere indicates the absence of trapped radiation belts and an ionosphere. Thus, the only charged particles of interest are those populating the interplanetary space traversed in Mercury's orbit. Design criteria monographs are being prepared on interplanetary and near-Earth charged particles.

2.5.1 Galactic Cosmic Rays

The interplanetary magentic field modulates the galactic cosmic ray fluxes observed near the Earth. In general it is believed that this modulation reduces the original interstellar fluxes more severely at lower energies, closer to the Sun, and during intervals of greater solar activity. In the absence of observations near Mercury, it is appropriate to specify galactic cosmic ray fluxes as between zero and the highest values observed near Earth. In the energy range $0.1 < E < 10^{10}$ GeV, the maximum flux Φ_E of particles with kinetic energy greater than E is approximated by

$$\Phi_E = A(E + E_o)^{-1.5} \tag{14}$$

where E_o is the rest energy of the particle and E is the kinetic energy in GeV (both E and E_o in GeV per nucleon for alpha-particles). Haffner's summary (ref. 48, fig. 2-3) specified $A \simeq 2.5$ cm^{-2}sec^{-1} for protons and $A \simeq 0.25$ cm^{-2}sec^{-1} for alpha-particles; Fanselow (ref. 49) specifies $A \simeq 0.02$ cm^{-2}sec^{-1} for electrons.

2.5.2 Solar Particle Events

Protons and alpha-particles of energies greater than 1 MeV are emitted sporadically by the Sun and have been detected by ground-based and spacecraft-borne instrumentation. Their fluxes near the Earth vary over several orders of magnitude in time, have both directional and isotropic components, and frequently can be associated with specific solar flares. Properties of sample events observed near the Earth are described in reference 50. The recent theoretical model by Englade (ref. 51) cites the important references on the complex processes of solar particle events. This literature shows that neither the probability of occurrence nor the associated particle fluxes and their variation can be estimated reliably. This is especially so, as close to the Sun as Mercury's orbit, where sporadic solar particle events can be expected to be more severe than near the Earth.

2.5.3 Solar Wind

Properties of the solar wind are summarized by Hundhansen (ref. 52). Protons and electrons have concentrations of approximately $5r^{-2}$ cm^{-3} (for r in AU) between 0.8 and 1.5 AU from the Sun on the basis of data from Mariner spacecraft. These particles are streaming radially

away from the Sun at speeds near 320 km/sec during quiet solar conditions with fluxes and energies of 1.6×10^8 r^{-2} cm^{-2} sec^{-1} and 0.5 keV for protons and 1.6×10^8 r^{-2} cm^{-2} sec^{-1} and 0.3 eV for electrons. Variations in solar activity result in temporary increases up to three in speed, ten in energy, and thirty in concentration and flux.

The applicable theory suggests that extrapolation on the basis of the foregoing r-dependence to the orbit of Mercury is reasonably conservative (ref. 52). Accordingly, for Mercury's eccentric orbit (r^{-2} ranging between 4.6 and 10.6, table VIII), the nominal range of concentration is 23 to 53 cm^{-3} and range of flux is 7×10^8 cm^{-2} sec^{-1} to 1.7×10^9 cm^{-2} sec^{-1}. The nominal speed and energy near Mercury are taken as identical to the values given in the preceding paragraph for near Earth. The factors of variation for concentration, flux, speed, and energy resulting from solar activity are taken for Mercury to be the same as near Earth.

2.6 Atmosphere

Theoretical and observational investigations have not determined conclusively whether any atmosphere exists on Mercury; Rasool et al. (ref. 24) and Belton et al. (ref. 53) review many of the pertinent discussions. The following three sections summarize their work and form the basis for the atmospheric models in section 2.6.4.

2.6.1 Pressure

The polarization measurements of Dollfus (refs. 54 and 55) were among the first observations to support quantitatively the reality of a Mercury atmosphere. These measurements indicated real differences from lunar dependences of the percentage of linear polarization on wavelength (green vs red) and location (cusp vs disk center). The apparent similarity of the lunar and Mercury surfaces (sec. 2.7) led to the conclusion that the polarization differences resulted from molecular scattering in a tenuous Mercury atmosphere for which a pressure of 1 mb was derived with a large uncertainty. Subsequent discussions have degraded this result by showing (1) that even one order-of-magnitude uncertainty is too definite (ref. 24), (2) that recent polarimetric studies of the moon and laboratory materials actually display excess polarization similar to Mercury's (ref. 56), and (3) that refined measurements of Mercury's polarization characteristics reduce the difference originally reported (ref. 35). After the discussion by Spinrad et al. (ref. 57) of the scattering power of various possible gaseous constituents, O'Leary and Rea (ref. 56) concluded that the sensitivity of the earlier polarimetric measurements requires a Mercury surface pressure less than 1 mb and that support for the existence of an atmosphere on this basis is not justified. The recent, more precise polarimetric results cited by Dollfus (ref. 35) have reduced the upper limit total pressure to 0.1 mb.

The apparent similarity of Mercury's surface properties to the moon's (sec. 2.7) is consistent with the hypothesis that their histories and environments are similar because of direct impact by solar wind and solar ultraviolet radiation. If these radiations reach Mercury's surface, a neglible atmosphere is implied. Also the discussion of the properties of the surface layers by Klein (ref. 45) concludes that the large value derived for the inverse thermal inertia

($[K\rho C]^{-1/2}$ Table VI) from the microwave observations requires that the surface pressure be less than 1 mb. This argument, based in part on the electrical behavior of laboratory rock powders, supports the conclusion that Mercury has no appreciable atmosphere.

Observations reporting temporary obscurations of surface features (ref. 58) and phase anomalies or projections of the horns (ref. 59) were near the limits of sensitivity (as are the spectroscopic observations, sec. 2.6.2) so are not strong evidence for an atmosphere or a basis for believable surface pressure estimates.

2.6.2 Temperature

Mercury's atmospheric temperature has not been observed, but there have been numerous discussions of hypothetical Mercury atmospheres with emphasis on temperatures and thermal properties. Articles by Rasool et al. (ref.24) and Belton et al. (ref. 53) are the most thorough because they consider solar ultraviolet radiation, infrared radiative transfer, conduction, convection, dissociation, and escape of atmospheric constituents, assumed to be primarily CO_2 and argon (cf. sec. 2.6.3). These processes control the temperature structure and through complex and tentative methods make possible the only available temperature estimates. They are summarized by the following statements.

In the lower atmosphere, for pressures > 0.1 mb, the surface temperature T forms the lower boundary condition and the temperature gradient should be approximately adiabatic until the value $(0.5)^{1/4}T$ is reached (ref. 24). Higher temperature gradients that would be required for conductive or radiative heat transport are unstable against convection, which would re-establish a nearly adiabatic gradient. At very low pressures ($\lesssim 10^{-8}$ mb), the exospheric temperatures depend strongly on the flux of solar ultraviolet radiation and thus vary diurnally and with the solar cycle. Temperatures suggested for the dayside exosphere with CO_2 assumed a major atmospheric constituent range between 980 and 2800 °K (refs. 24, 53 and 60). Under such circumstances the stability of any atmosphere as tenuous as required by the observational limits is hardly assured (ref. 53).

2.6.3 Composition

Spectroscopy has provided the basis for investigating the composition of Mercury's atmosphere as shown in table II. No spectral lines have been definitely associated with both Mercury and some known molecular species, however.

The detection of anomalous features near the center of the solar Fraunhofer lines $H\beta$ and $H\delta$ reflected from Mercury led Kozyrev (refs. 61 and 62) to propose an all-hydrogen atmosphere for Mercury, but most other researchers conclude that the anomalies have solar, terrestrial, or instrumental origins (ref. 63). Because hydrogen would escape quickly from Mercury at the exospheric temperatures cited in section 2.6.2, its absence from any Mercury atmospheric molecules is adopted herein. Kozyrev's arguments about the likelihood of a hydrogen atmosphere being cool and replenished from the solar wind are considered inconclusive. Likewise other lightweight molecules probably have escaped completely; according to Rasool et al. (ref. 24), those lighter than 23 g/mole cannot be present if the effective mean

TABLE II

SUMMARY OF SPECTROSCOPIC RESULTS FOR MERCURY

Wavelength (μm)	Molecule	Abundance (m-atm)	Pressure (mb)	Spectral Data Type	Reference	Remarks
0.4102(Hδ) 0.4861(Hβ)	H_2	0.8-80*	0.003-0.3*	photographic	Kozyrev (refs. 61 and 62)	Detection claimed*, abundance not estimated
0.4102(Hδ) 0.4861(Hβ)	H_2			photographic	Spinrad & Hodge (ref. 63)	Reality of detection in references 61 and 62 not accepted
"blue" $\sim$0.8				photographic	Dunham (ref. 64)	No Mercury lines detected
$\sim$0.8 $\sim$0.8 $\sim$0.8	H_2O O_2 CO_2	$<$30 μm** $<$ 1.0 $<$57	<0.05 <4.2	photographic	Spinrad et al. (ref. 57)	
1.049	CO_2	$<$ 5	<0.35	photoelectric	Belton et al. (ref. 53)	
1.203	CO_2	$<$ 1.0	<0.073	photographic	Bergstrahl et al. (ref. 65)	
1.203 1.2177	CO_2 CO_2	$<$ 0.2*** $<$ 0.58	<0.02*** <0.04	photographic	Bergstrahl et al. (ref. 65)	Band heads of CO_2 not detected
1.2177	CO_2	$<$ 1.4	<0.10	photographic	Bergstrahl et al. (ref. 65)	No Mercury lines detected
1.6	CO_2			IR Spectrometer	Binder & Cruikshank (ref. 66)	
1.6	CO_2	1.5-3.5*	0.11-0.26*	PbS photocell	Moroz (ref. 67)	Detection claimed*
2.12, 2.26 2.26-2.32 2.35 3.3	N_2O NH_3 CO CH_4	$<$ 0.02 $<$ 0.01 $<$ 0.1 $<$ 0.003	<0.0015 <0.0003 <0.005 <0.0001	PbS photocell	Moroz (ref. 67)	No Mercury lines detected

*Reality of detection questioned by other investigators listed at same wavelength.
**μm of precipitable water.
***Limit suspect because of nearby strong solar and terrestrial absorption lines.

exospheric temperature is 1000°K or higher. Thus, it is reasonable that other gases of molecular weight less than 40 have not been detected by spectroscopic analysis, which has yielded the upper abundance limits in table II.

Among gases whose molecular weight is greater than 44 g/mole, CO_2 is the most abundant in the atmospheres of Venus, Earth, and Mars; and its two elements are among the six most abundant in the Sun (ref. 8). Thus, it is likely to be present in Mercury's atmosphere. The spectroscopic evidence in table II except for the controversial claim by Moroz (ref. 67) yields 0.04 mb as the smallest reliable upper limit on the CO_2 partial pressure.

Field (ref. 68) has noted that the terrestrial ratio of the mass of atmospheric argon (also possibly heavy enough to be retained on Mercury) to the mass of the planet is approximately 10^{-8} with the argon presumably of radiogenic origin. The assumption that this mass ratio corresponds to the terrestrial value results in a partial pressure of argon on Mercury of 1.9 mb. This result suggests that there may be sufficient argon to constitute the difference between the CO_2 partial pressure limit (0.04 mb) and the total pressure limit (0.10 mb). A thin atmosphere of 40 per cent CO_2 and 60 per cent argon probably could remain cool enough through infrared emission to avoid the high temperatures derived by Belton et al. (ref. 53) that would cause the rapid loss of a mainly argon atmosphere.

2.6.4 Models

Because of most of the foregoing results, the simple conclusion that negligible atmosphere exists on Mercury is adopted as the nominal case. Therefore, a surface pressure of 10^{-15} atm or less (as on the Moon) is the only parameter required to describe the situation because this pressure is equivalent to a vacuum for spacecraft design and operations (ref. 36).

Nevertheless, to form a model atmosphere with upper limits for pressure and density, it is appropriate to combine the limiting data cited in sections 2.6.1 and 2.6.2 to obtain the maximum pressure and density at each altitide. The model uses the CO_2 partial pressure limit of 0.04 mb and the total surface pressure limit of 0.1 mb with argon accounting for the remaining pressure. The resulting composition is 0.60 A and 0.40 CO_2 by number and implies a mean molecular weight of 41.6 and an adiabatic lapse rate of -6°K/km on Mercury. The appropriate extreme of surface temperature is 700°K (sec. 2.7.3) and exosphere temperature 3000°K (sec. 2.6.2). The Earth's mean troposphere lapse rate is about 2/3 of the adiabatic (ref. 8). Thus, for Mercury a lapse rate of -4°K/km is appropriate up to the tropopause. At this level the temperature is $(0.5)^{1/4}$ (700°K) = 590°K. (The usual ratio of stratosphere to surface temperature has been used). In the upper atmosphere, the warmest temperatures cited in the theoretical literature (sec. 2.6.1) are approximately 250°K at the mesopause (pressure near 10^{-5} mb) and 3000°K at the critical level (pressure near 10^{-8} mb). With these considerations, the model atmosphere shown in table XIV (sec. 3.6) was derived on the basis of the relationships given in appendix B and constant lapse rates between the foregoing pressure-temperature points.

To account for night conditions, a model is specified which yields a still greater density in the region adjacent to the surface ($z < 8$ km). The surface pressure results from the

assumed pure argon atmosphere; the CO_2 would be frozen out at the prevailing temperature.

The foregoing models incorporate the greatest density that is consistent with observations. However, various other atmospheric compositions and regimes could be dominant that would make Mercury's atmosphere considerably less dense than predicted by the models. As stated before, the best estimate is that Mercury's atmosphere is completely neglible for design purposes.

2.7 Surface

2.7.1 Features

Surface detail is difficult to observe on Mercury for two reasons: (1) the angular extent of its disk is so small as seen from the Earth (<13 seconds of arc) that even high magnification does not yield resolution better than about one tenth of a radius which is comparable to that of the moon without magnification, and (2) the bright sky for daytime and long air path length for twilight observations lead to marginal contrast in observed features. These factors are partially responsible for the incorrect derivation of the rotation period from such observations before 1965 (sec. 2.1.3). Numerous observers interpreted their observations (recorded primarily in the form of drawings) in terms of a single sunlit hemisphere. (Schiaparelli, Fournier, Antoniadi, and Dollfus are widely known for this work.) These drawings and maps created from them, are summarized by Sandner (ref. 69). Since 1965 the drawings and some photographs obtained at the Pic du Midi and New Mexico Observatories have been reinterpreted on the basis of the 59-day rotation period. The most complete lists of such data have been given by Chapman (ref. 16) and Camichel and Dollfus (ref. 15). These authors have used the data on individual features and comparisons of drawings and photographs to support the 59-day period and prepare maps of Mercury's entire surface except the polar regions. The maps agree in most respects with one another; that from reference 15 is reproduced as figure 6 because it employs the recently adopted IAU longitude system (sec. 2.1.3). The features are positioned only to within about 10° accuracy and are not named. They differ in reflectivity by a real factor which, however, cannot be determined because of the impossibility of reliably calibrating drawings and plates made under the foregoing conditions of observation.

Radar observations reported by Goldstein (ref. 70) detected surface features but did not provide definite locations and properties. Smith et al. (ref. 71) find no evidence in their radar data for height variations on horizontal scales of 400 km or greater.

Therefore, there is insufficient basis from optical and radar observations to adopt variations in surface properties for different locations on the planet.

2.7.2 Physical Conditions

Measurements which relate to Mercury's surface properties indicate marginal differences at most between Mercury and the moon. The photometry (including the absolute and relative albedo, colors, contrast, and polarization and their dependences on wavelength and phase) is

almost indistinguishable from the moon's (sec. 2.4.2 and refs. 29, 30, 31, 32 and 35). Reflected radar signals show that Mercury's roughness and the ratio of its cross-section to its geometrical area are also indistinguishable from the moon's (sec. 2.7.3, ref. 72, and references in table III). Analysis of the microwave observations indicates that Mercury's electrical properties are similar to the moon's (sec. 2.7.3 and ref. 21); microwave observations coupled with infrared observations indicate that the thermal response of Mercury's surface is similar to that expected for the moon if placed in Mercury's orbit with its rotation (sec. 2.7.4, its references, and table V).

Theoretically, similarity between Mercury and the moon is to be expected on the basis that the qualitative theoretical considerations about the surface histories are the same. These concern the lack of an appreciable atmosphere (sec. 2.6) and the associated surface modification by meteorites (refs. 73, 74 and 75), solar wind (refs. 76 and 77), and solar ultraviolet radiation (refs. 24 and 53). The foregoing concept assumes that the original surface compositions and internally-generated orogenic processes were similar.

Therefore, the following sections assume that lunar values for the composition, mechanical properties, and topography can be applied directly to Mercury's surface. Much of material in these sections is taken from NASA SP-8023 (ref. 36) which has been corroborated by NASA SP-214 and SP-235 (refs. 78 and 79) that report Apollo 11 and 12 results.

2.7.2.1 Surface Composition

From the foregoing assumption of similar surface values for the moon and Mercury, the study of Apollo samples (ref. 80) provided pertinent data on composition of Mercury's rocks and soil. The minerals which make up the bulk of these samples are very similar to those found in terrestrial basalts (namely plagioclase, pyroxene, and ilmenite) and, less commonly, in anorthosites (primarily plagioclase)*. The minerals are primarily silicates and other oxides with the major differences from common terrestrial basalts being a larger fraction of ilmenite (containing iron and titanium oxides), the absence of ferric compounds, and the absence of moisture and hydrous minerals. Although Mercury's surface composition doubtless strongly depends on its local geological history, the absence of such data and photometric evidence (sec. 2.7.2) make it reasonable to accept the lunar surface composition as similar to Mercury's. One likely difference, however, would be an enhanced ratio of heavy metals, principally iron, in comparison to the Earth or moon, to make Mercury's surface composition compatible with its overall high mean density (sec. 2.1.2). The magnitude of this difference is indicated by Reynolds and Summers (ref. 81) in terms of overall iron mass fractions for which representative values of 0.68 for Mercury and 0.13 for the moon are obtained. According to Khodak (ref. 82), the heavy metals could be present on the surface in the form of a higher fraction of ilmenite than for the moon or of metallic iron and nickel.

*See Glossary, appendix C.

2.7.2.2 Soil Mechanical Properties

The mechanical properties of lunar soil have been measured remotely by Surveyor spacecraft, studied from the samples returned by the Apollo missions, and deduced from observations of astronauts and photographs of mobility and sinkage. The pre-Apollo and post-Apollo estimates agree in most important respects (refs. 36, 83 and 84). Because these properties are relatively numerous and complex, the lunar values are not discussed in detail here but simply tabulated in section 3.7 (table XV) and adopted for Mercury's surface. The results of Morrison (ref. 21) support the tabulated values of density and porosity because loosely-packed rock powders duplicate many of the properties required to explain the microwave data from Mercury. The other entries in table XV are from Costes et al. (ref. 83) and NASA SP-8023 (ref. 36). Appropriate definitions for properties listed in table XV are given in appendix C and are taken primarily from the soil mechanics texts by Bekker (ref. 85) and Scott (ref. 86).

2.7.2.3 Topography

The absence of shadows near the terminator, as observed from Earth, indicates that large-scale elevation differences are not significantly greater than on the moon. The maximum elevation differences of about 12 km (ref. 11) are reflected in the uncertainty ascribed to Mercury's radius (sec. 2.1.2). On smaller scales, relief or roughness is conventionally described in terms of the power spectral density function which is defined as the Fourier transform of the autocorrelation function of the surface elevation (ref. 85). Figure 7, adapted from reference 36, shows the range of power spectral density versus wavenumber on the moon which is adopted here as the roughness description for Mercury. The similarity in roughness is supported on scales between 10 and 100 cm by the radar data (table III). Slopes on the lunar surface are also specified in reference 36 from which figures 8 and 9 are adapted for Mercury.

Crater and block distributions are also specified in reference 36 for the moon. The distributions shown in figure 10 are taken directly from reference 36 for adoption here for Mercury's crater and block frequencies. The Apollo 12 mission (ref. 79) has confirmed these results for the moon and extended them to slightly smaller sizes for the craters. Craters outnumber blocks at all sizes shown for craters greater than 1 cm in diameter. For craters, the ratio of depth to diameter is less than 0.25, whereas for blocks the height is nominally 0.5 times the characteristic size (ref. 36). For blocks and particles, figure 11 from reference 36 shows the fraction of the surface area covered and indicates that the entire surface is covered with dust particles greater than 10 μm in size.

2.7.3 Electromagnetic Properties

Several radar observations have provided data on the electrical properties of Mercury's surface and the interaction of the surface with electromagnetic radiation. The original articles describing these observations (table III) indicate radar reflection properties for Mercury very

similar to those for the moon. These properties include a low radar reflectivity (ref. 87) which implies a high microwave emissivity. The latter is supported by the analyses of the microwave data obtained by the investigators listed in table I (sec. 2.4.4). On the basis of these data and appropriate theoretical considerations, several authors (references 21, 38, 39 and 88) have derived values for the electrical as well as thermal parameters of Mercury's surface layers (secs. 2.7.2.2 and 2.7.4). These results are based on the mean value and the amplitude and phase of the periodic variations of the brightness temperature as functions of wavelength and provide effective values for ϵ, $\tan \phi$, and δ/λ which are defined in appendices A and C. The ranges adopted in table IV for these parameters bracket not only the effective values cited in the literature but also variations likely to result from inhomogeneities. They are consistent with the composition and mechanical properties (sec. 2.7.2) and with corresponding ranges for the moon (ref. 21).

2.7.4 Temperature and Thermal Properties

Measurements of Mercury's emission in the infrared, particularly in the 8-14 μm region, have been interpreted in terms of the planet's surface temperature. Table V lists the temperature values so derived. All listed values are based on original observations except Soter's which is derived from Pettit and Nicholson's data. Night temperature values are difficult to obtain from the observations because the infrared energy received is susceptible to contamination by sunlight reflected from Mercury's illuminated crescent, the Earth's atmosphere, and the observing telescope. Nevertheless, the observations clearly indicate night surfaces are warmer than a permanently dark surface.

The microwave measurements of Mercury discussed in section 2.4.4 (table I) are also used to derive temperatures. The cited values depend on wavelength and are averages of physical temperatures at and below the surface and over the planet's disk. Thus, the microwave results have a smaller range of temperatures than the infrared ones.

The infrared and microwave temperature measurements have been supplemented by detailed theoretical analyses of the thermal and radio behavior of Mercury's surface layers of which only some highlights follow. Pettit and Nicholson (ref. 92) showed in calculations using the solar constant and Mercury's albedo that if the temperatures of sunlit surfaces are in equilibrium with the absorbed solar energy, they match the measured temperatures rather well. A detailed calculation is given by Soter and Ulrichs (ref. 20). They conclude that in thermal equilibrium the daytime temperature T of the sunlit surface is given by

$$T = T_p \left(\frac{r_p}{r}\right)^{1/2} (\cos Z)^{1/4} \qquad (15)$$

Here T_p equals 700 ± 25 °K, r_p equals (Mercury's perihelion distance) 0.3075 AU, r is its actual distance from the Sun, and Z (the zenith angle of the Sun) is less than 90°. Both the infrared and microwave data are consistent with temperatures calculated from equation (15). The uncertainty in T_p is that given by Morrison (ref. 21).

TABLE III

RADAR INVESTIGATIONS OF MERCURY

Reference	Wavelength (cm)	Chief Subject of Report
Carpenter & Goldstein (ref. 89)	12.5	Surface roughness
Goldstein (ref. 70)	12.5	Surface features (large scale)
Evans et al. (ref. 90)	23	Surface roughness
Ash et al. (ref. 5)	23, 70	Mass, radius, and ephemeris values
Kotel'nikov (ref. 91)	43	Reflectivity
Pettengill & Dyce (ref. 14)	70	Rotation rate
Pettengill et al. (ref. 87)	70	Cross-section and reflectivity
Smith et al. (ref. 71)		Surface features (large scale)

TABLE IV

ELECTROMAGNETIC PROPERTIES OF MERCURY'S SURFACE LAYERS

Property	Range of Values
Radar reflectivity	0.06 ± 0.03
Microwave emissivity	0.94 ± 0.03
Dielectric constant	$1.6 < \epsilon < 4$
Dielectric loss tangent	$0.002 < (tan\ \phi) < 0.013$
Ratios $\frac{\text{(electrical skin depth)}}{\text{(thermal skin depth) (wavelength)}}$	$0.5 < \frac{\delta}{\lambda} < 2.0\ \text{cm}^{-1}$

Surface twilight and night temperatures may be calculated from the theory of heat conduction if appropriate boundary conditions and thermal parameter values are assumed. For materials as dry and porous as Mercury's soil, conduction may occur simultaneously by contact (phonon transport) and radiation (photon transport). Analyses of these phenomena have been applied to Mercury by Soter and Ulrichs (ref. 20), Morrison (ref. 21), Winter and Saari (ref. 97), and Ulrichs and Campbell (ref. 98). When the geometrical circumstances of the solar radiation are taken into account (fig. 2, sec. 3.1) and lunar values for the thermal and electrical properties of the surface are employed, the variations of temperature theoretically predicted are consistent with the results of both the infrared and microwave observations which include part of Mercury's night hemisphere (tables I and V, and the references cited therein). Although some details of the variation of temperature with planetary latitude and longitude, depth below the surface, and time have been published (ref. 21), they are too complex to be practical for design criteria. Furthermore, although the foregoing results are reasonable for the planet as a whole, they may be unrealistic for particular locations because of surface inhomogenieties. The range from 90 to 200 °K brackets the observed values and those derived from the theory and is adopted here for the temperature of all surface points for which the Sun is invisible (night side or $Z > 90°$) or for which the temperature T predicted by equation (15) is less than 200 °K (near the terminator). Within this range, the higher temperatures are appropriate just after sunset and the lower ones from Mercury's midnight to dawn.

Table VI lists ranges of values for thermal properties which include those ascribed to Mercury by the foregoing authors and to the moon by NASA SP-8023 (ref. 36), Horai et al. (ref. 99), and Bastin et al. (ref. 100); the latter two references include results for lunar samples returned by Apollo 11. The ranges cited include both uncertainty and variations of characteristics with temperature and materials; they are deliberately large as contrasted with the range of effective values for the whole disk derived by Klein (ref. 88) and Morrison (ref. 21).

TABLE V

INFRARED OBSERVATIONS OF MERCURY
INTERPRETED AS SURFACE TEMPERATURES

Reference	Wavelength (μm)	Temperature (°K)	Interpretation
Pettit & Nicholson (ref. 92)	8–14	600	Subsolar point at mean distance from sun
Pettit (ref. 93)	8–14	613	Same
Soter (ref. 94)	8–14	180	Night quadrant, after sunset
Murray (ref. 95)	8–13	<150	Night hemisphere
Murdock & Ney (ref. 96)	3.75–11.3	522	Sunlit surface, including subsolar point
Murdock & Ney (ref. 96)	8.6	205	Sunlit crescent near terminator
Murdock & Ney (ref. 96)	11.8	111 ± 3	Night hemisphere

TABLE VI

THERMAL PARAMETER RANGES FOR
MERCURY CITED IN LITERATURE

Parameter	Range	Units
Specific heat	$0.07<C<0.24$	cal/g°K
Thermal conductivity	$2.5 \times 10^{-6}<K<4 \times 10^{-3}$	cal/cm sec°K
Inverse thermal inertia	$20<(K\rho C)^{-1/2}<2000$	$cm^2 sec^{1/2}$ °K/cal

3. CRITERIA

3.1 Physical Properties

Table VII gives values and uncertainties for Mercury's mass, radius, mean density, and rotation period, angular velocity, and axis inclination. The planet's solid surface is spherical, but local topographic variations (sec. 2.7.2) are responsible for the uncertainty associated with the radius. Table VIII gives some properties of Mercury's orbit. Mercury's position can be calculated from references 6 and 13. Figures 1 and 2 show the resonance relationship between Mercury's orbital and rotational motions.

TABLE VII

PHYSICAL PARAMETERS FOR MERCURY

Mass	$M_M = (3.32 \pm 0.02) \times 10^{23}$ kg
Radius	$R_M = 2435 \pm 6$ km
Mean density	$\bar{\rho} = 5.5 \pm 0.1$ g/cm^3
Period of rotation*	$T_r = 58.646 \pm 0.03$ days
Angular velocity of rotation*	$\omega_r = (1.2400 \pm 0.0006) \times 10^{-6}$ rad/sec
Inclination of rotational pole to normal of orbital plane	$< 10^\circ$

*Note that these quantities obey resonance relationships with the corresponding orbital quantities such that T_r equals two-thirds the period of orbital revolution T_o and ω_r equals three-halves the mean orbital angular velocity n.

3.2 Gravity Field

Table IX gives parameters and their uncertainties for Mercury's gravitational field.

3.3 Magnetic Field and Magnetosphere

Table X shows the ranges of Mercury's magnetic field and parameters of its magnetosphere. The field strength ranges between the interplanetary value of 10γ and the maximum dipole field strength, given by $2M_1/R^3$. The magnetosphere's boundary ranges from the planet's surface outward to a volume whose shape is roughly given by $R = R_1 (4\text{-}\cos\theta)/3$ where θ is the angle from the solar direction.

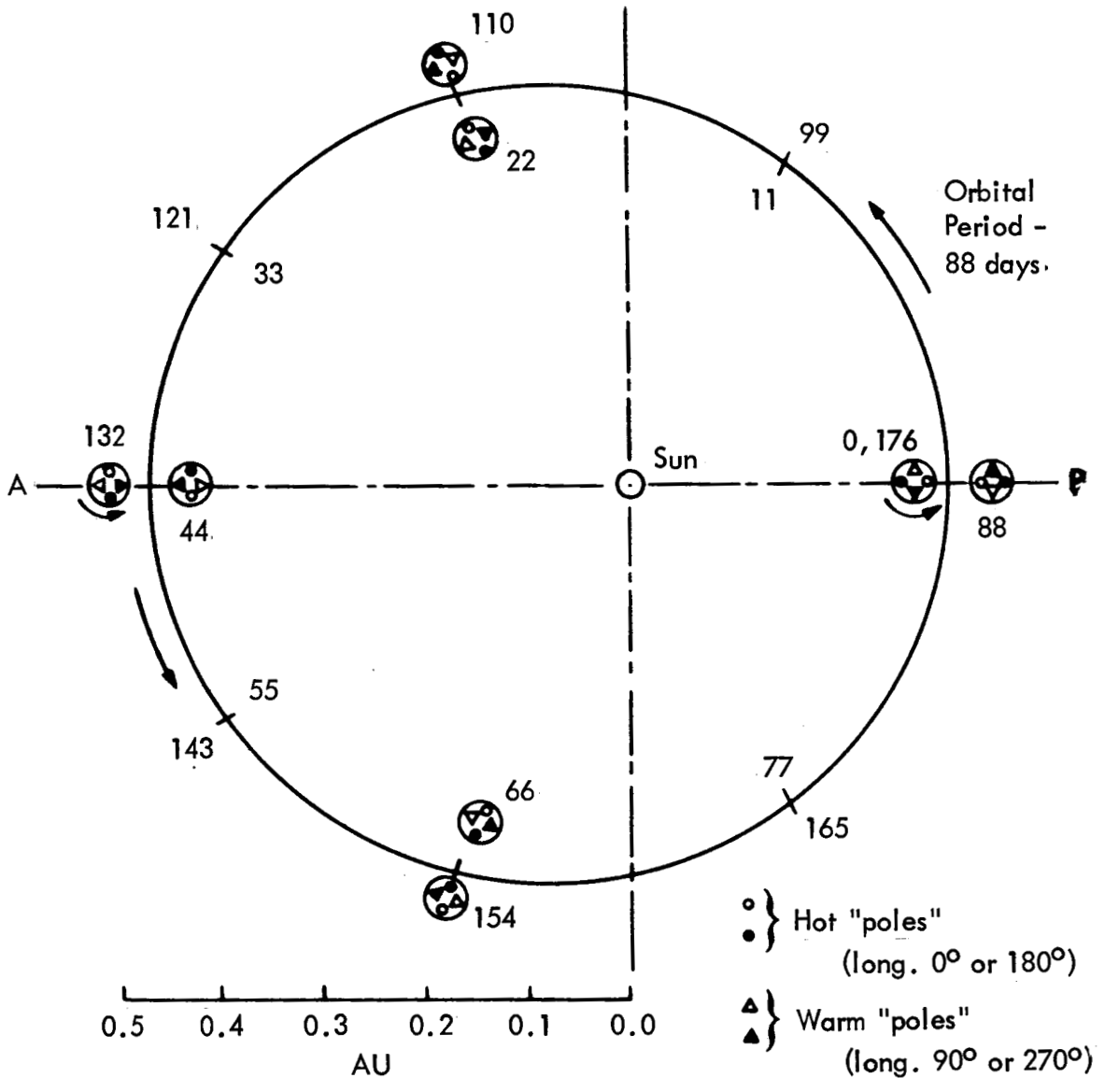

Figure 1. - The spin-orbit coupling of Mercury. The plane of the figure is that of Mercury's orbit, viewed from the north pole, with the directions of perihelion (P) and aphelion (A) shown. The symbols within the circles (representing the planet) show the changing directions of equatorial surface points at the four longitudes on Mercury that are labelled hot and warm "poles" per section 2.1.3. Cycle starts at perihelion, and each 11 day interval is marked for the complete cycle of 176 days, the length of Mercury's "day".

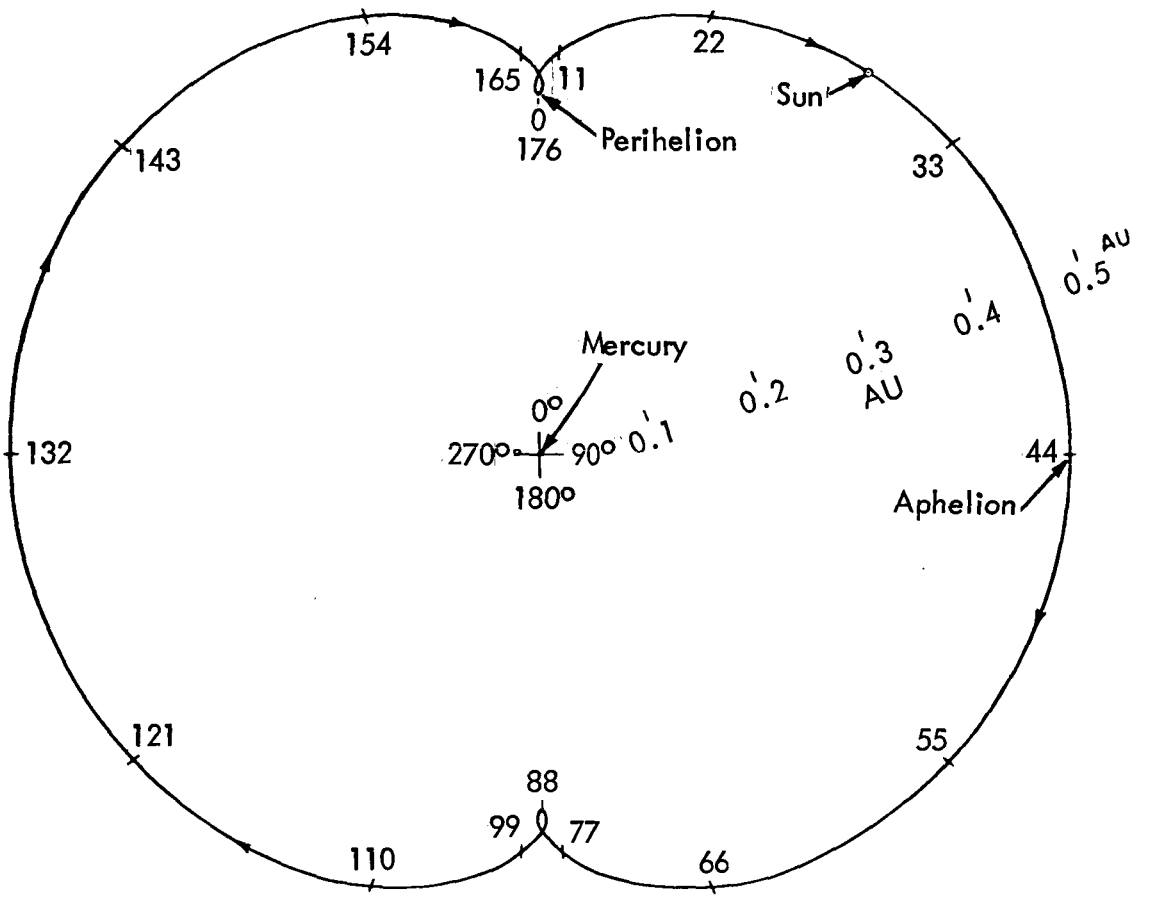

Figure 2. - The Sun's motion in Hermocentric longitude. The plane of the figure is that of Mercury's orbit, viewed from the north pole, and the Mercury longitude system is that adopted by the IAU. Points on the Sun's path are labelled at 11-day intervals, and the Sun's apparent motion is clockwise except for parts of the loops at perihelion (ref. 20).

TABLE VIII

SELECTED PARAMETERS OF MERCURY'S ORBIT

Parameter	Value
Semi-major axis	$a = 0.3871$ AU
Inclination to ecliptic	$i = 7^\circ$
Eccentricity	$e = 0.2056$
Perihelion distance	$a(1-e) = 0.3075$ AU
Aphelion distance	$a(1+e) = 0.4667$ AU
Sidereal period	$T_o = 87.969$ days
Synodic period	115.88 days
Mean motion (orbital angular velocity)	$n=2\pi/T_o = 8.267 \times 10^{-7}$ rad/sec
Maximum angular velocity	$n(1-e)^{-2} = 1.310 \times 10^{-6}$ rad/sec
Minimum angular velocity	$n(1+e)^{-2} = 5.688 \times 10^{-7}$ rad/sec

TABLE IX

GRAVITATIONAL PARAMETERS OF MERCURY

Gravitational potential	$\psi = -(9.10 \pm 0.07\ km^2/sec^2)\ (R_M/R)$
Escape velocity at distance R	$V_e = (4.27 \pm 0.02\ km/sec)\ (R_M/R)^{1/2}$
Period of Keplerian orbit of semi-major axis a	$T_a = (84.5 \pm 0.6\ min)\ (a/R_M)^{3/2}$
Surface acceleration of gravity	$g = 374 \pm 4\ cm/sec^2$

TABLE X

PARAMETERS OF MERCURY'S MAGNETIC FIELD

Upper limit of magnetic dipole moment	$M_1 = 4 \times 10^{23}$ gauss-cm^3
Interplanetary field strength and local lower limit	10 γ
Upper limit of equatorial surface field strength	$M_1/R_M{}^3 = 0.028$ gauss
Upper limit of magnetosphere's sunward extent	$R_1 < 2R_M = 4870$ km

3.4 Electromagnetic Radiation

The expressions in table XI specify the intensities and fluxes of electromagnetic radiation from the major sources, Mercury itself and the Sun at wavelengths between 1 Å and 100 cm. Radiation beyond these limits is expected to be too weak to affect spacecraft design. The Sun's contribution is described in terms of its spectral irradiance P_λ in NASA SP-8005 (ref. 1). For light reflected from Mercury, the phase function $\phi(a)$ and the geometric albedo $p(\lambda)$ are given by

$$log\ \phi(a) = \frac{a}{250}\left[3.8 + \frac{a}{100}\ (-2.73 + \frac{a}{50})\right] \qquad (16)$$

and

$$\log p(\lambda) = (-0.94 \pm 0.07) + (0.25 \pm 0.05)(2-\lambda^{-1}) \quad . \tag{17}$$

Here the phase angle a is expressed in degrees and the wavelength λ in μm. The average albedo of the surface is $0.12 \times 2^{\pm 1}$.

The light from other planets is given by the expression for the apparent magnitude

$$m = (m_o \pm 0.3) + 5 \log(r\Delta) + (0.03 \pm 0.02)a$$

for r and Δ in AU (appendices A and C) when the values for m_o in table XII are used. Star brightnesses are given in standard catalogs on magnitude scales. When there is shadowing from both the Sun and Mercury, the minimum integrated flux is 4.6×10^{-10} watt/cm^2.

Mercury's radio intensities and fluxes are also given in table XI where the brightness temperature T_B is shown as a function of wavelength per figure 3. Equivalently, the radio flux is more simply given by the standard Rayleigh-Jeans formula

$$F_\nu = 2kT_B\Omega/\lambda^2 \quad .$$

Here Ω is the smaller of Mercury's solid angle or the antenna beam solid angle.

3.5 Charged Particles

Mercury is not expected to have significant charged particle populations in the absence of trapped radiation belts or an ionosphere. Of the externally-imposed charged particles, the galactic cosmic rays may be less than their near-Earth fluxes, but the near-Earth values form a good upper limit and are given in table XIII. Energetic solar protons and the solar wind are both considerably more severe near Mercury than near Earth and are given in table XIII. Monographs on near-Earth and interplanetary charged particles are being prepared.

3.6 Atmosphere

Nominally and for design purposes, Mercury has neglible atmosphere, i.e., its surface pressure is less than 10^{-15} atmosphere like the Moon. The upper limit density atmosphere consistent with the observations and theory is composed of 60 percent argon and 40 percent carbon dioxide by number and has a molecular weight of 41.6 grams/mole. The values of altitude z, temperature T, pressure P, density ρ, pressure scale height H_p, and density scale height H_ρ are given in table XIV for sunlit and dark periods from the surface up to the level where the mass density drops to about 10^{-16} g/cm^3. Profiles of temperature, pressure, and density versus altitude are given in figures 4 and 5 for sunlit and dark upper limit density models. The sunlit model has greater density at all altitudes except adjacent to the surface ($z < 8$ km) where the dark model has greater density.

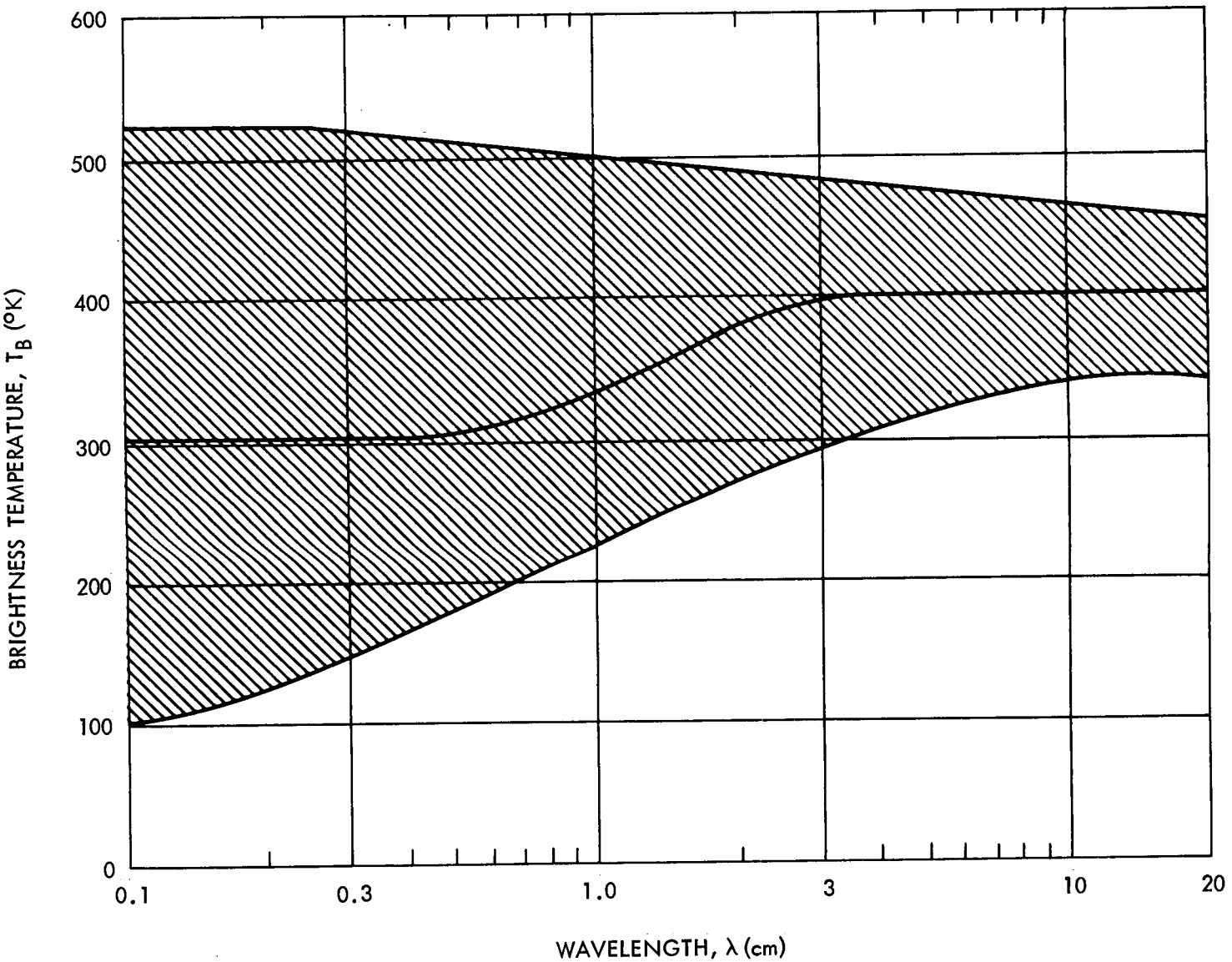

Figure 3. – The range of brightness temperature T_B for Mercury. The central line represents the nominal dependence of T_B on wavelength λ, and the shaded area includes the uncertainties and time variations.

TABLE XI

ELECTROMAGNETIC RADIATION NEAR MERCURY

	Direct Sunlight*	Sunlight Reflected from Mercury**	Mercury Thermal and Radio Emission***
Intensity	$I_\lambda = \dfrac{P_\lambda}{(6.8 \times 10^{-5}\ \text{sterad})}$	$0 < I_\lambda < \dfrac{p(\lambda)\ P_\lambda}{r^2\,(\pi\ \text{sterad})}$	$I_\lambda = B_\lambda(T)$
Flux	$F_\lambda = P_\lambda / r^2$	$0 < F_\lambda < \dfrac{p(\lambda)\phi(a)}{r^2\ (R/R_M)^2}\ P_\lambda$	$F_\lambda = \dfrac{\pi B_\lambda(T)}{(R/R_M)^2}$
Integrated Flux	$0.62 < F < 1.43\ \dfrac{\text{watt}}{\text{cm}^2}$	$0 < F < \dfrac{0.35}{(R/R_M)^2}\ \dfrac{\text{watt}}{\text{cm}^2}$ (average albedo = $0.12 \times 2^{\pm 1}$)	$\dfrac{0.0004}{(R/R_M)^2} < F < \dfrac{1.4}{(R/R_M)^2}\ \dfrac{\text{watt}}{\text{cm}^2}$

*Beyond shadow of Mercury, take solar spectral irradiance P_λ, given in NASA SP-8005 (ref. 1), and use distance r from Sun in AU.

**Applicable except for conditions of specular reflection of sunlight; then the entires in column 1 are appropriate upper limits. Expressions for $p(\lambda)$ and $\phi(a)$ are in section 3.4, P_λ is from NASA SP-8005 (ref. 1) and r is distance from Sun in AU.

***For $\lambda < 0.1$ cm, the range of T is that of the physical temperature of the observed surface (sec. 3.7); for $\lambda > 0.1$ cm the range of T is that of the brightness temperature T_B shown in Figure 3.

TABLE XII

PHOTOMETRIC PARAMETERS FOR THE SUN, MOON, AND PLANETS

	Photometric Passband Parameters*				
	U	B	V	R	I
Effective wavelength (μm)	0.353	0.448	0.554	0.690	0.820
Apparent magnitude of the Sun (m_e)	-28.04	-28.18	-28.81	-29.26	-29.55
Absolute magnitude of –					
Mercury (m_o)	**	+0.57	-0.36	-1.21	-1.73
Venus (m_o)	-2.97	-3.47	-4.29	**	**
Earth (m_o)	**	-3.67	-3.87	**	**
Moon (m_o)	+1.59	+1.13	+0.21	-0.59	-1.05
Mars (m_o)	+0.42	-0.16	-1.52	-2.64	-3.02
Jupiter (m_o)	-7.94	-8.42	-9.25	-9.75	-9.72
Saturn (m_o)***	-7.26	-7.84	-8.88	**	**
Uranus (m_o)	-6.35	-6.63	-7.19	-7.04	-6.24
Neptune (m_o)	-6.25	-6.46	-6.87	-6.54	-5.74
Pluto (m_o)	+0.06	-0.21	-1.01	-1.64	-1.92

*See appendix A of Newburn, R. L., and Gulkis, S., 1971, "A Brief Survey of the Outer Planets Jupiter, Saturn, Uranus, Neptune, Pluto, and Their Satellites," Jet Propulsion Laboratory TR 32-1529.

**Data not available.

***Can vary with ring inclination up to one magnitude less, i.e., brighter, than specified.

TABLE XIII

PARAMETERS OF CHARGED PARTICLES NEAR MERCURY

Parameter	Energy or Velocity	Concentration or Flux
Galactic cosmic rays	$0.1 < E < 10^{10}$ GeV*	$\Phi_E = A\,(E + E_o)^{-1.5}$** For — electrons ($E_o$ = 0.00051 GeV): $0 \leqslant A \leqslant 0.02$ protons (E_o = 0.938 GeV): $0 \leqslant A \leqslant 2.5$ alphas (E_o = 0.942 GeV/nucleon): $0 \leqslant A \leqslant 0.25$
Energetic solar particles	$E > 1$ MeV	Sporadic proton and alpha-particle fluxes of uncertain severity but greater than near Earth. (Sample events are described in NASA TR R-169.)
Solar Wind Protons***	V_s = 320 km/sec E = 0.5 keV	N = 38 ±15 cm^{-3} Φ = (1.2 ±0.5) X 10^9 cm^{-2} sec^{-1}
Solar Wind Electrons***	V_s = 320 km/sec E = 0.3 eV	N = 38 ±15 cm^{-3} Φ = (1.2 ±0.5) X 10^9 cm^{-2} sec^{-1}

*Kinetic energy E in GeV (for alphas in GeV/nucleon).
**Flux Φ of particles with kinetic energy >E in cm^{-2} sec^{-1}.
***Temporary increases up to factors of three in the speed V_s, ten in the energy E, and thirty in the concentration N and flux Φ may occur, most likely during peak solar activity.

TABLE XIV

MERCURY UPPER LIMIT DENSITY ATMOSPHERIC MODELS

Sunlit (noon)						Dark			
z (km)	T (°K)	P (mb)	ρ (g/cm^3)	H_p (km)	H_ρ (km)	T (°K)	P (mb)	ρ (g/cm^3)	H_p or H_ρ (km)
0.0	700	0.1000	7.15×10^{-8}	37.4	47.6	100	600×10^{-2}	2.89×10^{-7}	5.56
5.0	680	0.0873	6.42×10^{-8}	36.4	46.2	84	2.26×10^{-2}	1.29×10^{-7}	4.67
10.0	660	0.0759	5.76×10^{-8}	35.3	44.9	84	7.05×10^{-3}	4.04×10^{-8}	4.67
15.0	640	0.0658	5.14×10^{-8}	34.2	43.5	84	2.42×10^{-3}	1.38×10^{-8}	4.67
20.0	620	0.0567	4.57×10^{-8}	33.1	42.2	84	8.28×10^{-4}	4.74×10^{-9}	4.67
25.0	600	0.0486	4.05×10^{-8}	32.1	40.8	84	2.84×10^{-4}	1.63×10^{-9}	4.67
27.5	590**	0.0450	3.81×10^{-8}	31.5	40.1	84	1.66×10^{-4}	9.52×10^{-10}	4.67
30.0	585	0.0415	3.55×10^{-8}	31.3	34.8	84	9.73×10^{-5}	5.58×10^{-10}	4.67
40.0	566	0.0300	2.65×10^{-8}	30.3	33.7	84	1.14×10^{-5}	6.55×10^{-11}	4.67
50.0	547	0.0214	1.96×10^{-8}	29.2	32.6	84	1.34×10^{-6}	7.70×10^{-12}	4.67
60.0	528	0.0151	1.43×10^{-8}	28.2	31.4	84	1.58×10^{-7}	9.04×10^{-13}	4.67
70.0	509	0.0105	1.04×10^{-8}	27.2	30.3	84	1.86×10^{-8}	1.06×10^{-13}	4.67
80.0	490	0.00725	7.41×10^{-9}	26.2	29.2	84	2.18×10^{-9}	1.25×10^{-14}	4.67
100.0	452	0.00327	3.62×10^{-9}	24.1	26.9	84	3.00×10^{-11}	1.72×10^{-16}	4.67
120.0	413	0.00138	1.67×10^{-9}	22.1	24.6				
140.0	375	0.000532	7.10×10^{-10}	20.1	22.3				
160.0	337	0.000186	2.76×10^{-10}	18.0	20.0				
180.0	299	5.72×10^{-5}	9.58×10^{-11}	16.0	17.8				
200.0	261	1.50×10^{-5}	2.87×10^{-11}	13.9	15.5				
205.5	250**	1.00×10^{-5}	2.00×10^{-11}	13.4	9.8				
210.0	280	7.29×10^{-6}	1.30×10^{-11}	15.0	11.0				
225.0	381	3.10×10^{-6}	4.07×10^{-12}	20.4	15.0				
250.0	549	1.12×10^{-6}	1.02×10^{-12}	29.4	21.6				
275.0	717	5.34×10^{-7}	3.72×10^{-13}	38.4	28.2				
300.0	886	2.97×10^{-7}	1.68×10^{-13}	47.3	34.8				
350.0	1222	1.21×10^{-7}	4.97×10^{-14}	65.3	48.0				
400.0	1559	6.17×10^{-8}	1.98×10^{-14}	83.3	61.3				
500.0	2232	2.28×10^{-8}	5.10×10^{-15}	119.3	87.7				
600.0	2905	1.09×10^{-8}	1.88×10^{-15}	155.3	114.2				
614.19	3000**	1.00×10^{-8}	1.67×10^{-15}	160.4	160.4				
700.0	3000	5.856×10^{-9}	9.76×10^{-16}	160.4	160.4				
800.0	3000	3.14×10^{-9}	5.23×10^{-16}	160.4	160.4				
900.0	3000	1.68×10^{-9}	2.81×10^{-16}	160.4	160.4				
1000.0	3000	9.02×10^{-10}	1.50×10^{-16}	160.4	160.4				

*For an isothermal atmosphere $\frac{d \log T}{d \log P} = \beta = 0$, $H_\rho = H_p$ (app. B).

**At these levels the lapse rate dT/dz changes value.

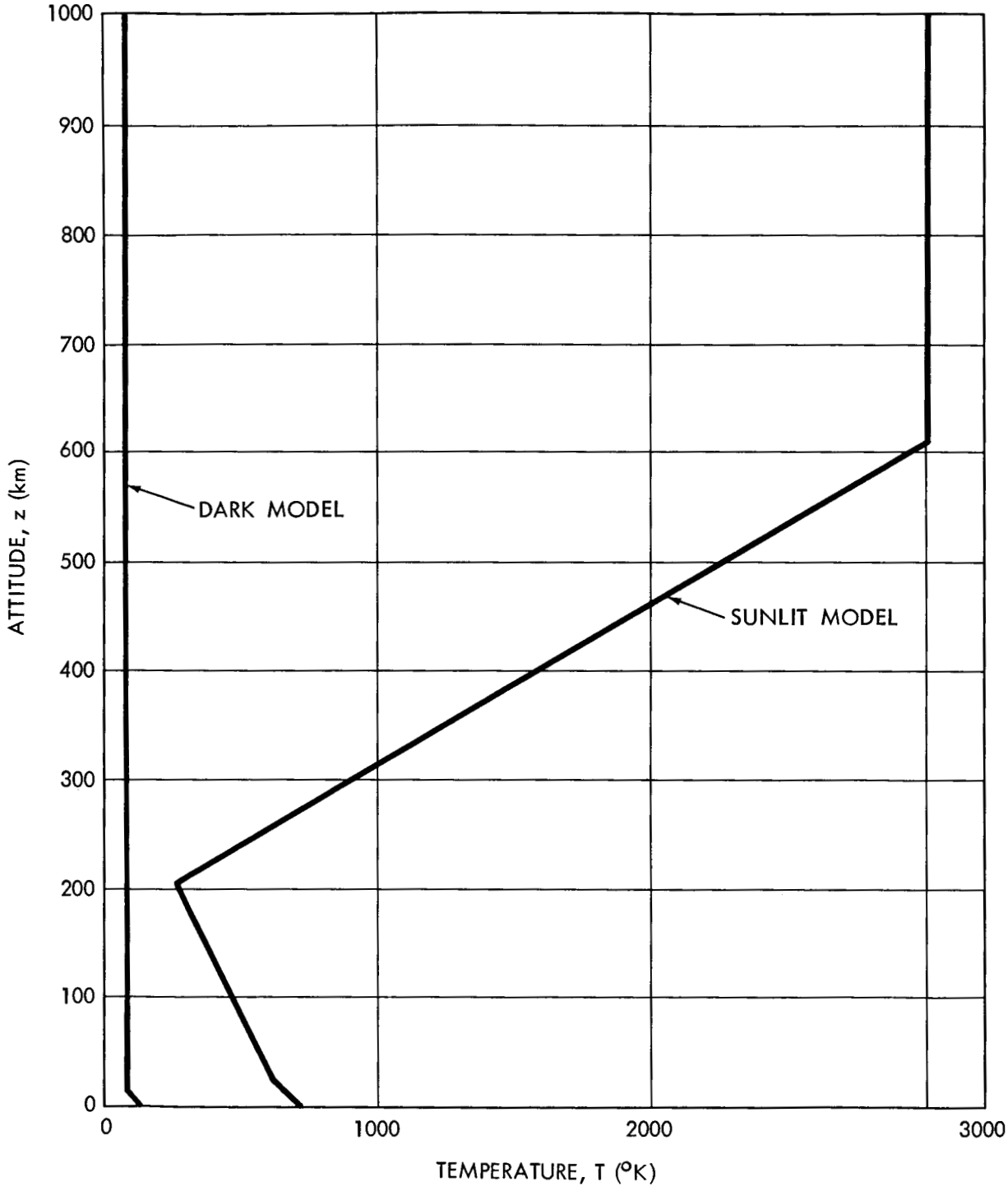

Figure 4. - Range of temperatures between dark and sunlit profiles versus altitude for the Mercury upper limit density model.

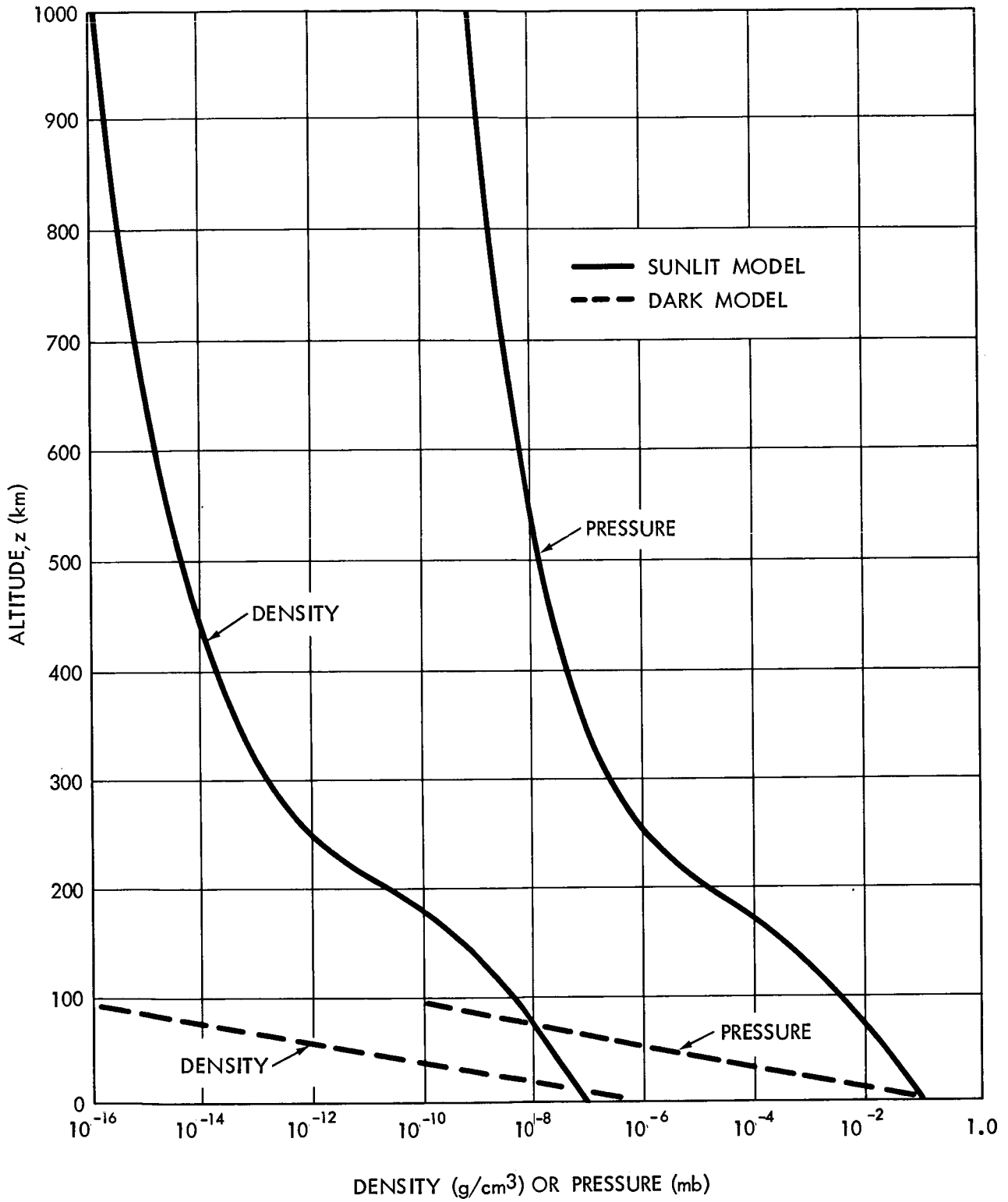

Figure 5. - Dark and sunlit model profiles of density and pressure versus altitude for upper limit density atmospheres.

3.7 Surface

Figure 6 shows the light and dark areas on Mercury's surface. The surface relief deviates less than ±6 km from that of a perfect sphere. Other topographical, roughness, crater, and particle distributions and associated ranges are shown in figures 7 through 11. Composition, soil mechanics, thermal properties, and electromagnetic properties are given in tables XV and XVI.

TABLE XV

SOIL MECHANICS PROPERTIES FOR MERCURY

Properties	Symbols, Values, Units
Bulk density Porosity Specific gravity	1.8 ±0.2 g/cm^3 0.35 to 0.53 3.1 to 3.4 g/cm^3
Grain size	2 to 60 μm
Cohesion Adhesion Static Bearing capacity (y = penetration depth in cm)	0.02 to 0.2 Newton/cm^2 (nominal 0.05 N/cm^2) 0.0025 to 0.01 N/cm^2 (1.0 ±0.4)y Newton/cm^2
Angle of internal friction	31 to 39 degrees
Effective coefficient of friction (metal to soil or rock)	0.4 to 0.8

TABLE XVI

COMPOSITION, THERMAL PROPERTIES, AND
ELECTROMAGNETIC PROPERTIES OF MERCURY'S SURFACE

Properties	Description/Values
Composition	Basalts (plagioclase pyroxene, enriched in ilmenite) and, less commonly, anorthosities (primarily plagioclase); possible metallic iron also present.
Temperature	$T = (388 \pm 15^\circ K)[(\cos Z)/r^2]^{1/4}$ if $T > 200^\circ K$; otherwise $90^\circ K \leq T \leq 200^\circ K$ near terminator and at night ($Z > 90^\circ$).
Specific heat Thermal conductivity Inverse thermal inertia	$0.07 \leq C \leq 0.24$ cal/g° K $(2.5 \times 10^{-6}) \leq K \leq (4 \times 10^{-3})$ cal/cm sec° K $20 < (K\rho C)^{-1/2} < 2000$ cm^2 sec$^{1/2}$° K/cal
Radar reflectivity Microwave emissivity	0.06 ± 0.03 0.94 ± 0.03
Dielectric constant Loss tangent $\frac{\text{(Electrical skin depth)}}{\text{(Thermal skin depth)(Wavelength)*}}$	$1.6 \leq \epsilon \leq 4$ $0.002 \leq (\tan \phi) \leq 0.013$ $0.5 < \frac{\delta}{\lambda} < 2.0$ cm^{-1}

*Wavelength of electromagnetic radiation of interest.

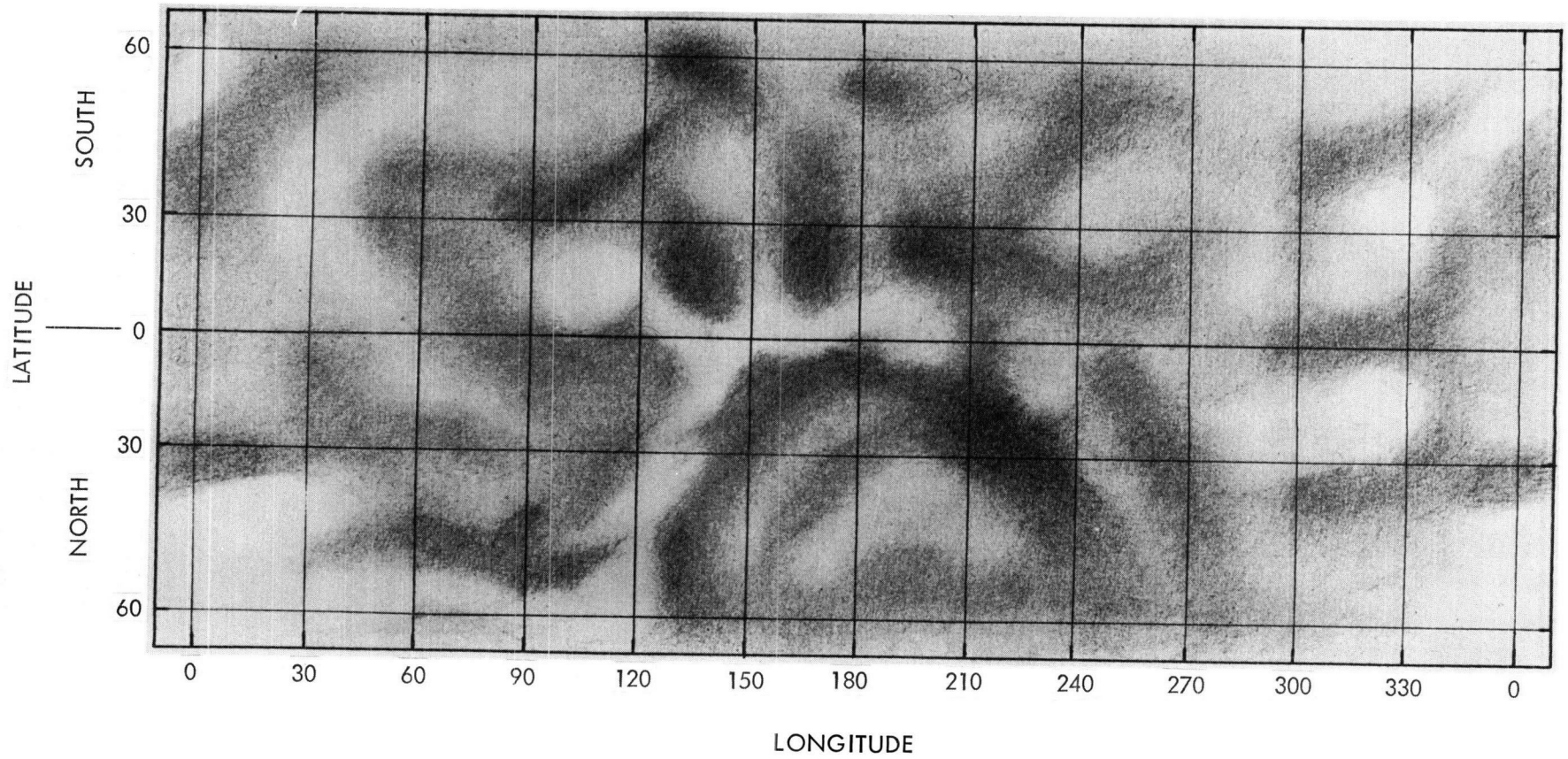

Figure 6. – Map of the surface features of Mercury from Camichel and Dollfus (ref. 15.). The Mercator projection is used, South is at the top, and the longitude system is that adopted by the IAU (sec. 2.1.3).

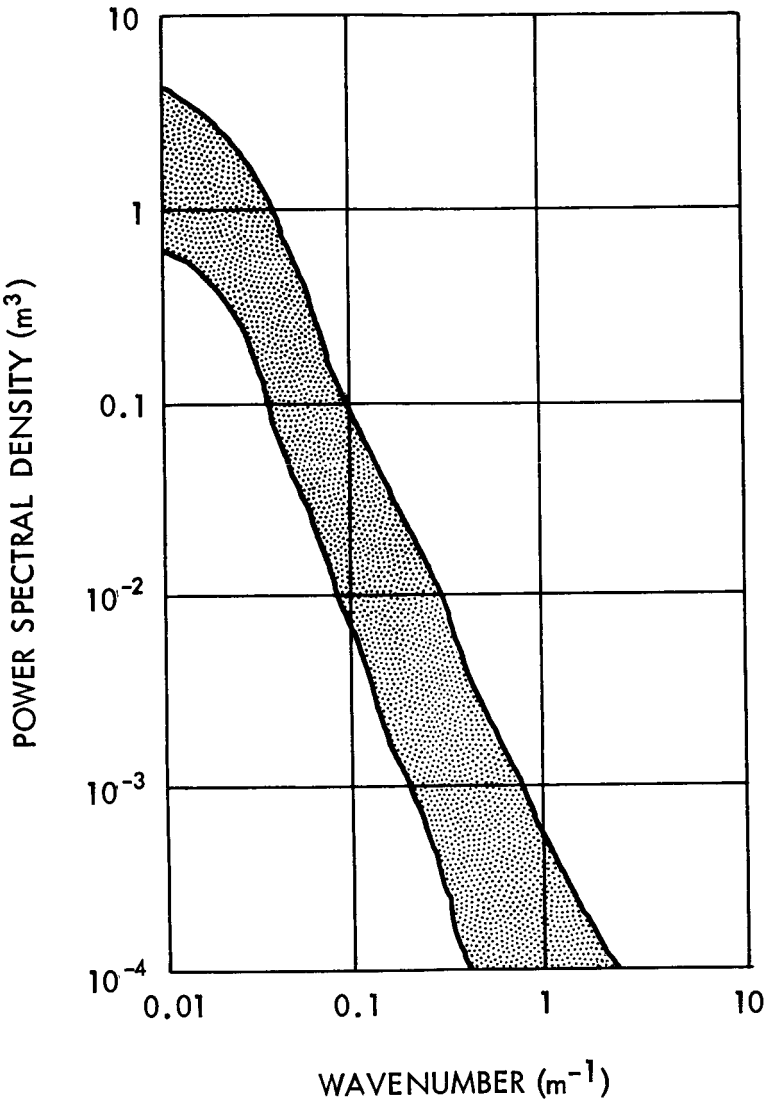

Figure 7. - Roughness of Mercury's surface, given by the power spectral density of the elevation as a function of the wavenumber (ref. 36).

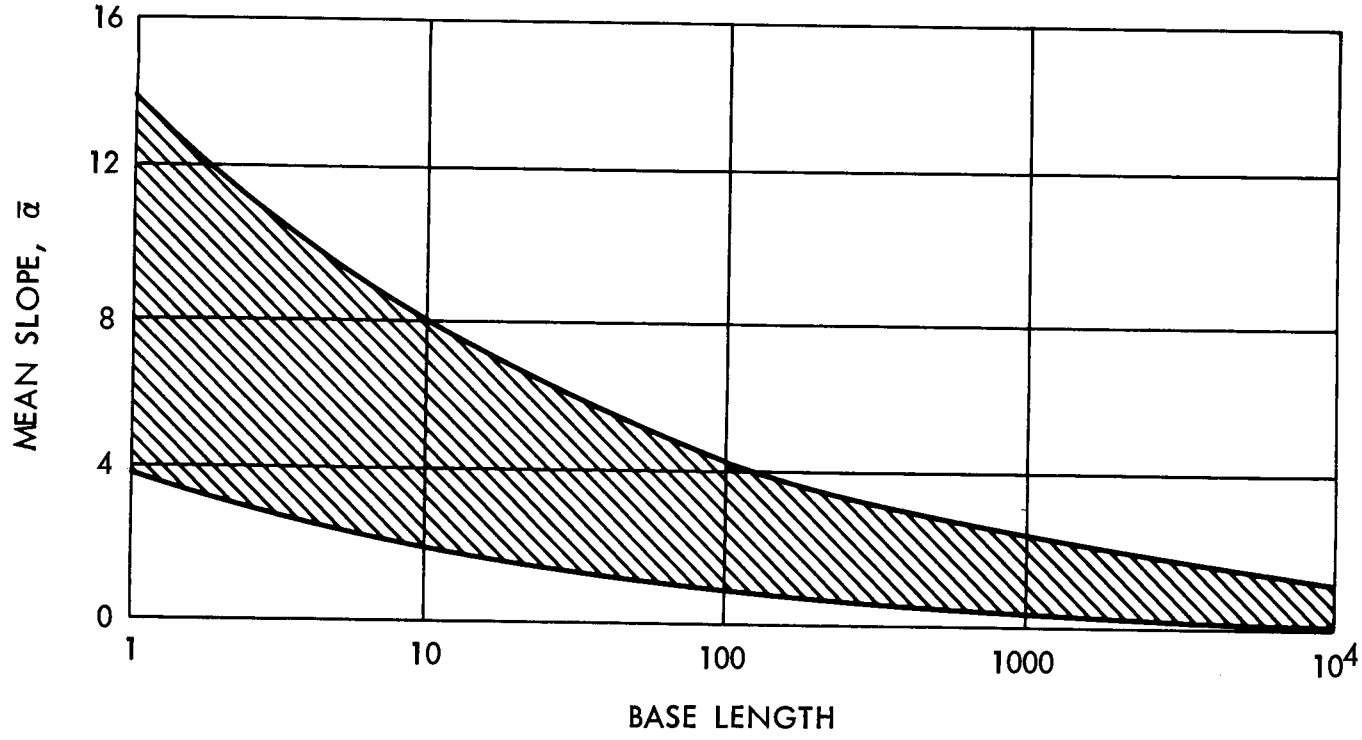

Figure 8. - Variation of mean slope of Mercury's surface with horizontal base length (ref. 36).

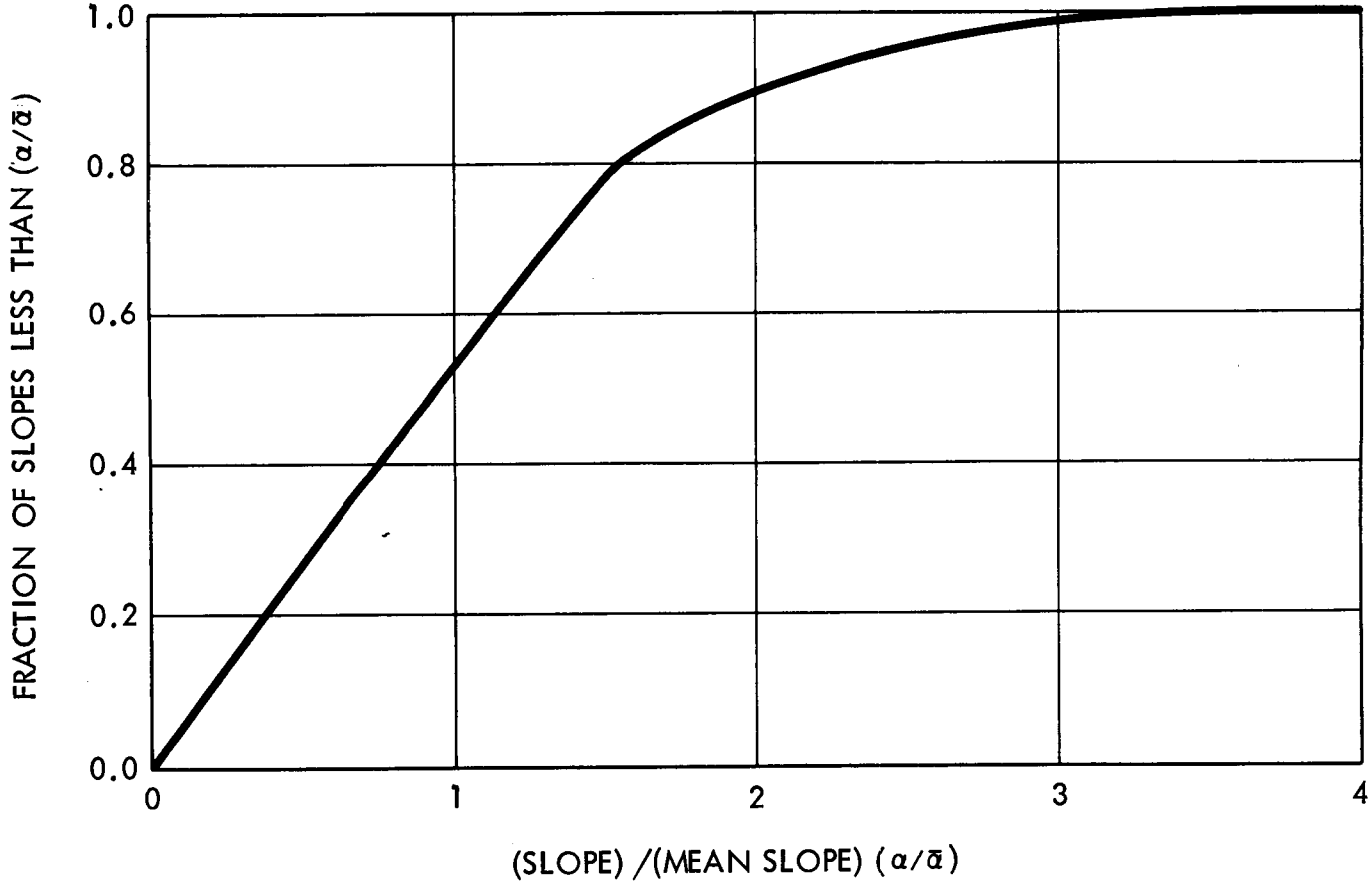

Figure 9. - Relative distribution of slopes on Mercury's surface for use with figure 8 (ref. 36).

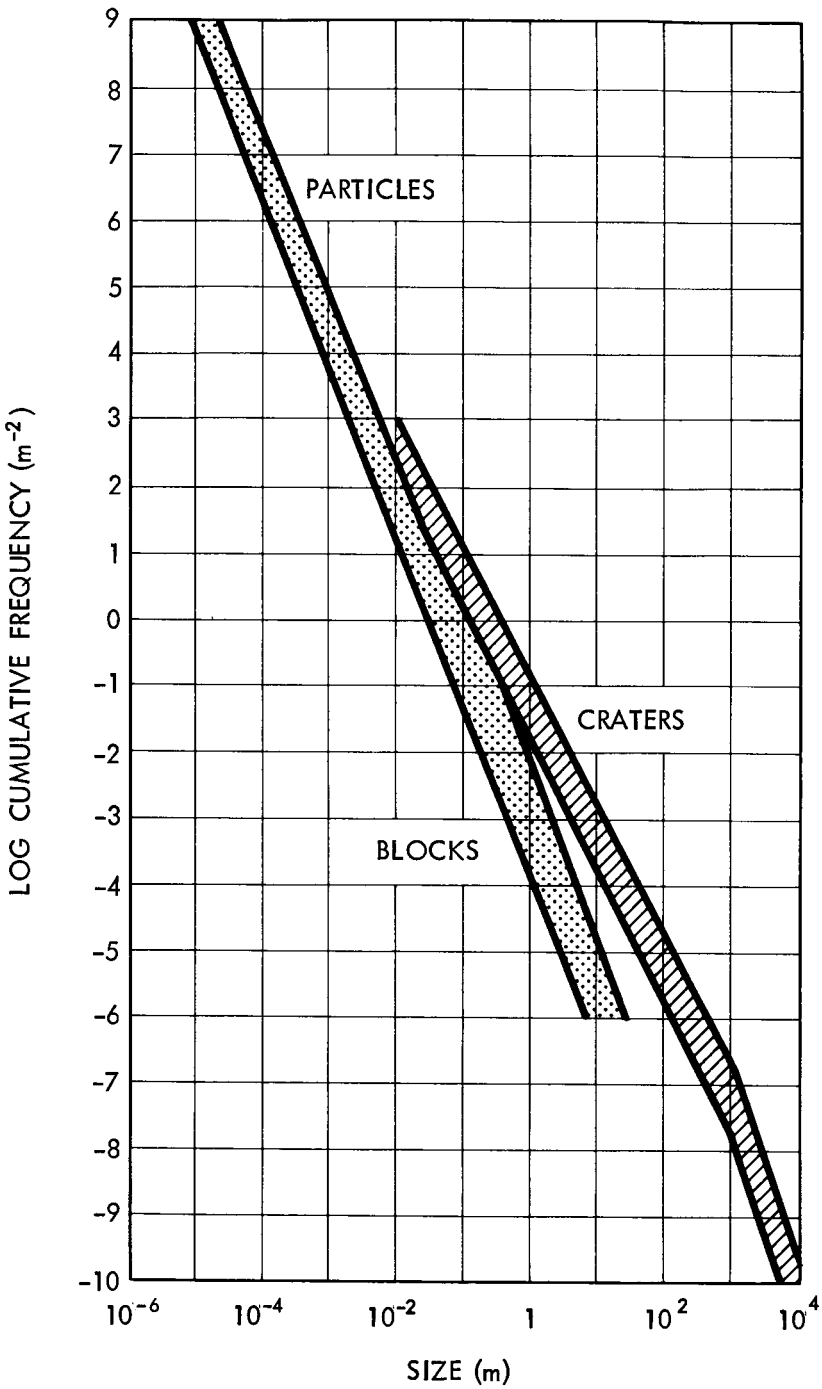

Figure 10. – Number per unit area of blocks, particles, and craters larger than specified characteristic size for the surface of Mercury (refs. 36, 83 and 84).

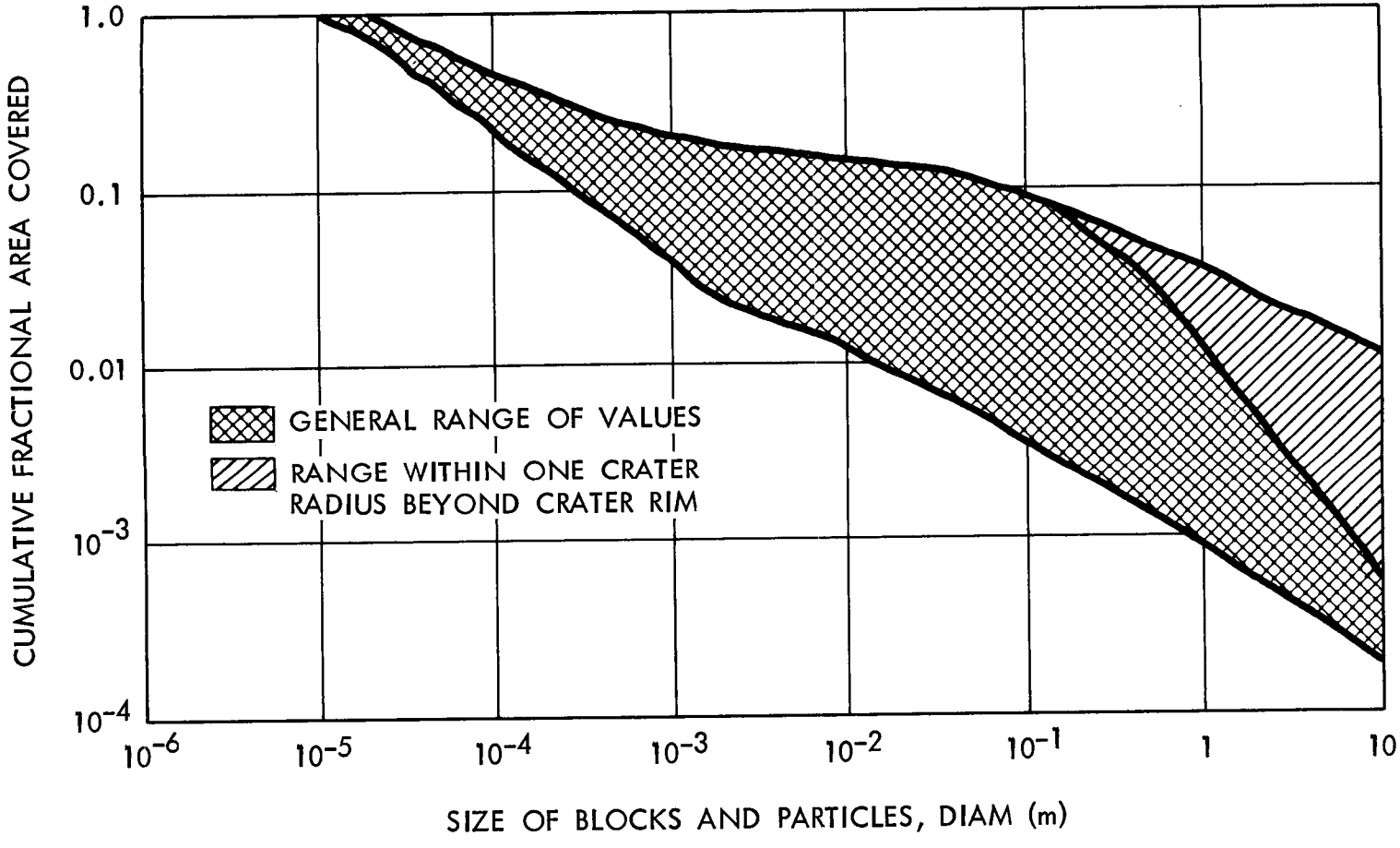

Figure 11. - Fraction of surface area covered by blocks and particles larger than specified characteristic size for the surface of Mercury (ref. 36).

REFERENCES

1. Anon.: Solar Electromagnetic Radiation. NASA SP-8005, Revised, May 1971.

2. Anon.: Magnetic Fields–Earth and Extraterrestrial. NASA SP-8017, March 1969.

3. Anon.: Meteoroid Environment Model–1970 (Interplanetary and Planetary). NASA SP-8038, October 1970.

4. Klepczynski, W. J.; Seidelman, P. K.; and Duncombe, R. L.: The Masses of the Principal Planets. Presented at IAU Colloquium No. 9, Heidelberg, 12-15 August, 1970.

5. Ash, M. E.; Shapiro, I. I.; and Smith, W. B.: Astronomical Constants and Planetary Ephemerides Deduced from Radar and Optical Observations. Astronom. J., vol. 72, no. 3, 1967, pp. 338-350.

6. Melbourne, W. G.; Mulholland, J. D.; Sjogren, W. L.; and Sturms, F. M.: Constants and Related Information for Astrodynamic Calculations, 1968. Technical Report 32-1306, Jet Propulsion Laboratory, Pasadena, 1968.

7. Null, G. W.; and Lieske, J. H.; Astronomical Constants from Observations of the Inner Planets and Icarus. Am. Astronomical Society Bulletin, vol. 1, no. 4, 1969, pp. 356-357.

8. Allen, C. W.: Astrophysical Quantities (Second Edition). Athlone Press, Univ. of London, 1963.

9. de Vaucouleurs, G.; Geometric and Photometric Parameters of the Terrestrial Planets. Icarus, vol. 3, 1964, pp. 187-235.

10. Dollfus, A.: Diamètres dés Planètes et Satellites, Surfaces and Interiors of Planets and Satellites. Dollfus, A., ed., Academic Press, New York, chapter 2, 1970, p. 46.

11. Wright, F. E.; Wright, F. H.; and Wright, H.; "The Lunar Surface: Introduction", The Moon Meteorites and Comets. Middlehurst, B. M., and Kuiper, G. P., eds., Solar System, vol. 4, Univ. of Chicago Press, chapter 1, 1963, pp. 1-56.

12. Liu, H. -S.: On the Figure of the Planet Mercury. Celestial Mechanics, vol. 1, no. 1, 1969, 144-149.

13. American Ephemeris and Nautical Almanac. U.S. Government Printing Office.

14. Pettengill, G. H.; Dyce, R. B.: A Radar Determination of the Rotation of the Planet Mercury. Nature, vol. 206, no. 4990, 1965, p. 1240.

15. Camichel, H.; and Dollfus, A.: La Rotation et la Cartographie de la Planete Mercure. Icarus, vol. 8, no. 2, 1968, pp. 216-226.

16. Chapman, C. R.: Optical Evidence on the Rotation of Mercury. Earth and Planetary Science Letters, vol. 3, no. 4, 1967, pp. 381-385.

17. Smith, B. A.; and Reese, E. J.: Mercury's Rotation Period: Photographic Confirmation. Science, vol. 162, No. 3859, 1968, pp. 1275-1277.

18. Liu, H.-S.; and O'Keefe, J. A.: Theory of Rotation for the Planet Mercury. Science, vol. 150, 1965, p. 1717.

19. Colombo, G.; and Shapiro, I. I.: The Rotation of the Planet Mercury. Astrophys. J., vol. 145, 1966, p. 296.

20. Soter, S.; and Ulrichs, J.: Rotation and Heating of the Planet Mercury. Nature, vol. 214, no. 5095, 1967, pp. 1315-1316.

21. Morrison, D.; Thermophysics of the Planet Mercury. Space Science Reviews, vol. 11, no. 2/3, 1970, pp. 271-307.

22. O'Leary, B. T.; Campbell, M. J.; and Sagan, C.: Lunar and Planetary Mass Concentrations. Science, vol. 165, no. 3894, 1969, pp. 651-657.

23. Kern, T. W.; and Vestine, E. H.: Magnetic Field of the Earth and Planets. Space Science Reviews, vol. 3, 1963, p. 136.

24. Rasool, S. I.; Gross, S. H.; and McGovern, W. E.: The Atmosphere of Mercury. Space Sci. Reviews, vol. 5, no. 5, 1966, pp. 565-584.

25. Good, R. C.: The Magnetosphere of the Planet Mercury as a Scattering Center for Solar Flare Protons. AIAA Paper 67-150, 1967, 8 pp.

26. Reiffel, L.: Trapped Radiation Estimates for the Other Planets. McCormack, B. M., ed., Radiation Trapped in the Earth's Magnetic Field, D. Reidel Publ. Co., Dordrecht, Holland, 1966, pp. 256-262.

27. Shatten, K. H.; Wilcox, J. M.; and Ness, N. F.: A Model of Interplanetary and Coronal Magnetic Field. J. Solar Physics, vol. 6, 1969, pp. 442-455.

28. Thekaekara, M. P.: Proposed Standard Values of the Solar Constant and the Solar Spectrum. J. Environmental Science, vol. 13, no. 4, 1970, pp. 6-9.

29. Harris, D. L.: Photometry and Colorimetry of Planets and Satellites, Planets and Satellites. Kuiper, G. P., and Middlehurst, B. M., eds., Solar System, vol. 3, Univ. of Chicago Press, chapter 8, 1961, pp. 272-342.

30. Irvine, W. M.; Simon, T.; Menzel, D. H.; Pikoos, C.; and Young, A. T.: Multicolor Photoelectric Photometry of the Brighter Planets, III. Observations from Boyden Observatory Astronom. J., vol. 73, no. 9, 1968, pp. 807-828.

31. Hämeen-Anttila, K. A.: Surface Photometry of the Planet Mercury. Ann. Acad. Sci. Fennicae A, vol. VI, no. 252, 1967.

32. Hämeen-Anttila, K. A.; Pikkarainen, T.; and Carmichel, H.: Photometric Studies of the Planet Mercury. The Moon, vol. 1, 1970, p. 440.

33. de Vaucouleurs, G.: Photomètrie des Surfaces Planétaires, Surfaces and Interiors of Planets and Satellites. Dollfus, A., ed., Academic Press, New York, chapter 5, 1970, p. 226.

34. Minnaert, M.: General Conclusions, La Physique des Planètes. Memoires de la Société Royale des Sciences de Liège, vol. 24, 1962, p. 597.

35. Dollfus, A.: Résultats Récents sur les Planètes Mercure, Vénus et Mars, Obtenus par les Observations Astronomiques au Sol. La Recherche Spatiale, vol. 7, no. 1, 1968, pp. 1-12.

36. Anon.: Lunar Surface Models. NASA SP-8023, May 1969.

37. Linsky, J. L.: Models of the Lunar Surface Including Temperature-Dependent Thermal Properties. Icarus, vol. 5, 1966, p. 606.

38. Morrison, D.; and Klein, M. J.: The Microwave Spectrum of Mercury, Astrophys. J., vol. 160, no. 1, 1970, pp. 325-332.

39. Epstein, E. E.; Dworetsky, M. M.; Fogarty, W. G.; Montgomery, J. W.; and Cooley, R. C.: Mercury: Epileth Physical Parameters and a Hermocentric Longitude Dependence of its 3.3-mm Radiation. Radio Science., vol. 5, no. 2, 1970, pp. 401-409.

40. Epstein, E. E.; Oliver, J. P.; Schorn, R. A.; Soter, S. L.; and Wilson, W. J.: Mercury: Observations of the 3.4-Millimeter Radio Emission. Science, vol. 157, no. 3796, 1967, pp. 1550-1552.

41. Golovkov, V. K.; and Losovskii, B. Ya.: Measurements of the Phase Dependence of the 0.8-cm Radio Emission of Mercury, and Some Properties of its Surface Layer. Soviet Astronomy-AJ, vol. 12, no. 2, 1968, pp. 229-302.

42. Welch, W. J.; Thornton, D. D.; and Lohman, R.: Observations of Jupiter, Saturn, and Mercury at 1.53 cm. Astrophys. J., vol. 146, no. 3, 1966, pp. 799-809.

43. Kaftan-Kassim, M. A.; and Kellermann, K. I.: Measurements of the 1.9 cm Thermal Radio Emission from Mercury. Nature, vol. 213, no. 5073, 1967, pp. 272-273.

44. Howard, W. E.; Barrett, A. H.; and Haddock, F. T.: Measurements of Microwave Radiation from the Planet Mercury. Astrophys. J., vol. 136, 1962, pp. 995-1004.

45. Klein, M. J.: Mercury: Recent Observations at 3.75-cm Wavelength – Summary, Radio Science, vol. 5, no. 2, 1970, pp. 397-400.

46. Kellermann, K. I.: 11-cm Observations of the Temperature of Mercury. Nature, vol. 205, no. 4976, 1965, pp. 1091-1092.

47. Woolley, R.v.d.R.: Planetary Co-ordinates for the years 1960-1980. Her Majesty's Stationery Office, London, 1958.

48. Haffner, J. W.: Radiation and Shielding in Space. Academic Press, New York, 1967.

49. Fanselow, J. L.: The Primary Cosmic-Ray Electron Spectrum between 0.09 and 8.4 BeV in 1965. Astrophys. J., vol. 152, no. 3, 1968, p. 783.

50. McDonald, F. B., ed.: Solar Proton Manual. NASA TR R-169, 1963.

51. Englade, R. C.: A Computational Model for Solar Flare Particle Propagation. Thesis, University of Chicago, 1970.

52. Hundhansen, A. J.: Direct Observations of Solar Wind Particles. Space Science Reviews, vol. 8, no. 5/6, 1968, p. 690.

53. Belton, M. J. S.; Hunten, D. M.; and McElroy, M. B.: A Search for An Atmosphere on Mercury. Astrophys. J., vol. 150, no. 3, 1967, pp. 1111-1124.

54. Dollfus, A.: Observations of an Atmosphere Around the Planet Mercury. Comptes Rendus, vol. 231, 1950, pp. 1430-1432.

55. Dollfus, A.: Visual and Photographic Studies of Planets at the Pic du Midi. Solar System, vol. 3, chapter 15, 1961, pp. 534-571.

56. O'Leary, B. T.; and Rea, D. G.: On the Polarimetric Evidence for an Atmosphere on Mercury. Astrophys. J., vol. 148, no. 1, 1967, pp. 249-253.

57. Spinrad, H.; Field, G. B.; and Hodge, P. W.: Spectroscopic Observations of Mercury. Astrophys. J., vol. 141, 1965, pp. 1155-1160.

58. Antoniadi, E. M.: La Planète Mercure. Gauthier-Villars, Paris, 1934.

59. Haas, W. H.: A Ten-Year Study of Mercury and its Atmosphere, Popular Astronomy. Vol. 55, 1947, pp. 137-148.

60. Vaughan, O. H.: Model Atmospheres of Mercury. J. Spacecraft and Rockets, vol. 6., no. 10, 1969, pp. 1171-1175.

61. Kozyrev, N. A.: The Atmosphere of Mercury. Sky and Telescope, vol. 27, 1964, pp. 339-341.

62. Kozyrev, N. A.: Letter to the Editor. Sky and Telescope, vol. 30, 1965, p. 360.

63. Spinrad, H.; and Hodge, P. W.: An Explanation of Kozyrev's Hydrogen Emission Lines in the Spectrum of Mercury. Icarus, vol. 4, 1965, pp. 105-108.

64. Dunham, T.: Spectroscopic Observations of the Planets at Mount Wilson, The Atmospheres of the Earth and Planets. Kuiper, G. P., ed., revised edition, Univ. of Chicago Press, chapter 11, 1952, pp. 288-305.

65. Bergstralh, J. T.; Gray, L. D.; and Smith, H. J.: An Upper Limit for Atmospheric Carbon Dioxide on Mercury. Astrophys. J., vol. 149, no. 3, 1967, pp. L137-139.

66. Binder, A. B.; and Cruikshank, D. P.: Mercury: New Observations of the Infrared Bands of Carbon Dioxide. Science, vol. 155, no. 3765, 1967, p. 1135.

67. Moroz, V. I.: Infrared Spectrum of Mercury. Soviet Astronomy–AJ, vol. 8, no. 6, 1965, pp. 882-889.

68. Field, G. B.: Atmosphere of Mercury. Astronom. J., vol. 67, 1962, pp. 575-576.

69. Sandner, W.: The Planet Mercury, Faber & Faber, London, 1963.

70. Goldstein, R. M.: Mercury: Surface Features Observed During Radar Studies, Science, vol. 168, no. 3930, 1970, pp. 467-469.

71. Smith, W. B.; Ingalls, R. P.; Shapiro, I. I.; and Ash, M. E.: Surface-Height Variations on Venus and Mercury. Radio Science, vol. 5, no. 2, 1970, pp. 411-423.

72. Muhleman, D. O.: Radar Scattering from Venus and Mercury at 12.5 cm. J. Research Radio Science, vol. 69D, no. 12, 1965, pp. 1630-1631.

73. Hodge, P.: Interactions of the Planet Mercury with Interplanetary Material, La Physique des Planètes. Memoires de la Société Royale des Sciences de Liège, vol. 24, 1962, pp. 261-268.

74. Hodge, P. W.: The Atmosphere of the Planet Mercury. AGU Transactions, vol. 45, no. 45, no. 4, 1964, p. 631.

75. Sharonov, V.: Dust Covers on the Surface of Planets and Satellites. Life Sciences and Space Research II, North Holland Publ. Co., Amsterdam, 1964, pp. 171-177.

76. Field, G. B.: "The Atmosphere of Mercury", The Origin and Evolution of Atmospheres and Oceans. John Wiley & Sons, New York, 1964, pp. 269-278.

77. Sagan, C.; and Morrison, D.: The Planet Mercury. Science J., vol. 4, no. 12, 1968, pp. 72-77.

78. Anon.: Apollo 11 Preliminary Science Report. NASA SP-214, 1969.

79. Anon.: Apollo 12 Preliminary Science Report. NASA SP-235, 1970.

80. Wood, J. A.: The Lunar Soil, Scientific American, vol. 223, no. 2, 1970, pp. 14-23.

81. Reynolds, R. T.; and Summers, A. L.: Calculations on the Composition of the Terrestrial Planets. J. Geophysical Research, vol. 74, no. 10, 1969, p. 2494.

82. Khodak, Yu. A.: Hermesology—Geology of Mercury. Izvestiya Akad. Nauk CCCP, Seriya Geologiya, no. 10, 1969, pp. 136-142 (U. S. Dept. of Commerce, Joint Publications Research Service 48346, No. 217, Nov. 28, 1969).

83. Costes, N. C.; Carrier, W. D.; Mitchell, J. K.; and Scott, R. F.: Apollo 11 Soil Mechanics Investigation. NASA SP-214, 1969, pp. 85-122.

84. Scott, R. F.; Carrier, W. D.; Costes, N. C.; and Mitchell, J. K.: Mechanical Properties of the Lunar Regolith. NASA SP-235, 1970, pp. 161-182.

85. Bekker, M. G.: Off-the-Road Locomotion. Univ. of Michigan Press, Ann Arbor, 1960.

86. Scott, R. F.: Principles of Soil Mechanics. Addison-Wesley, Reading, Mass., 1963.

87. Pettengill, G. H.; Dyce, R. B.; and Campbell, D. B.: Radar Measurements at 70 cm of Venus and Mercury. Astron. J., vol. 72, no. 3, 1967, pp. 330-337.

88. Klein, M. J.: Mercury: Measurements of Variations in the Microwave Disk Temperature. (to be published).

89. Carpenter, R. L.; and Goldstein, R. M.: Radar Observations of Mercury. Science, vol. 142, 1963, p. 381.

90. Evans, J. V.; Brockelman, R. A.; Henry, J. C.; Hyde, G. M.; Kraft, L. G.; Reid, W. A.; and Smith, W. W.: Radio Echo Observations of Venus and Mercury at 23 cm Wavelength, 1965, Astronom. J., vol. 70, no. 7, 1965, pp. 486-501.

91. Kotel'nikov, V. A.: Radar Probes of the Planet Mercury. Doklady Akad. Nauk SSSR, vol. 147, no. 6, 1962, pp. 1320-1323.

92. Pettit, E.; and Nicholson, S. B.: Radiation from the Planet Mercury. Astrophys. J., vol. 83, 1936, p. 84-102.

93. Pettit, E.: "Planetary Temperature Measurements", Planets and Satellites. Kuiper, G. P., and Middlehurst, B. M., eds., Solar System, vol. 3, Univ. of Chicago Press, chapter 10, 1961, pp. 400-428.

94. Soter, S. L.: Mercury – Infrared Evidence for Nonsynchronous Rotation. Science, vol. 153, 1966, pp. 1112-1113.

95. Murray, B. C.: Infrared Radiation from the Daytime and Nighttime Surfaces of Mercury. American Geophysical Union Transactions, vol. 48, no. 1, 1967, pp. 148-149.

96. Murdock, T. L.; and Ney, E. P.: Mercury: The Dark-Side Temperature. Science, vol. 170, no. 3957, 1970, pp. 535-537.

97. Winter, D. F.; and Saari, J. M.: A Particulate Thermophysical Model of the Lunar Soil. Astrophys. J., vol. 156, no. 3, 1969, pp. 1135-1151.

98. Ulrichs, J.; and Campbell, M. J.: Radiative Heat Transfer in the Lunar and Mercurian Surfaces. Icarus, vol. 11, no. 2, 1969, pp. 180-188.

99. Horai, K.; Simmons, G.; Kanamori, H.; and Wones, D.: Thermal Diffusivity and Conductivity of Lunar Material. Science, vol. 167, no. 3918, 1970, pp. 730-731.

100. Bastin, J. A.; Clegg, P. E.; and Fielder, G.: Infrared and Thermal Properties of Lunar Rock. Science, vol. 167, no. 3918, 1970, pp. 728-730.

APPENDIX A
SYMBOLS*

A	cosmic ray **flux** parameter (sec. 2.5.1)
a	semi-major axis of elliptical orbit (secs. 2.2, 3.1)
B	blue **magnitude** (table XII)
$B_\lambda(T)$	blackbody **intensity** per unit wavelength as a function of temperature (sec. 2.4.3)
C	specific heat of soil (tables VI, XVI)
E	charged particle kinetic energy (sec. 2.5 and table XIII)
E_o	cosmic ray rest energy in GeV (sec. 2.5.1)
e	orbital eccentricity (table VIII)
F	**integrated flux** of electromagnetic radiation (table XI)
F_λ	**flux** of electromagnetic radiation per unit wavelength (table XI)
F_ν	**flux** of radio radiation per unit frequency (sec. 2.4.4)
G	universal constant of gravitation, 6.668×10^{-8} g cm^3 sec^{-2} (sec. 2.2)
g	surface acceleration of gravity (sec. 2.2)
H_p	pressure scale height (table XIV, app. B)
H_ρ	density scale height (table XIV, app. B)
I	infrared **magnitude** (table XII)
I_λ	**intensity** of electromagnetic radiation per unit wavelength (table XI)
i	orbital inclination to **ecliptic** (table VIII)
K	**thermal conductivity** (tables VI and XVI)
k	Boltzmann's constant, 1.380×10^{-16} erg/°K (sec. 2.4.4)
M_1	magnetic dipole moment (sec. 2.3)
M_M	mass of Mercury (sec. 2.1.1)
$M_\odot$	mass of Sun (sec. 2.1.1)
m	apparent **magnitude** (sec. 2.4.5)
$m_\odot$	apparent **magnitude** of the Sun (sec. 2.4.2)
m_o	absolute visual **magnitude** (sec. 2.4.5)
N	concentration of solar wind protons or electrons (table XIII)
n	mean orbital angular velocity (table VIII)

*Words in bold face are defined in Glossary (app. C).

P	atmospheric pressure (sec. 3.6, app. B)
P_A	atmospheric pressure at altitude z_A (app. B)
P_λ	solar spectral irradiance, per unit wavelength (sec. 2.4.1)
$p(\lambda)$	**geometric albedo**, as a function of wavelength (sec. 2.4.2)
R	red **magnitude** (table XII)
R	distance from center of Mercury (sec. 2.4 and table XI)
R_M	radius of Mercury (sec. 2.1.2)
R_1	sunward boundary of Mercury's magnetosphere (sec. 2.3)
R_g	universal gas constant (app. B)
r	distance from the Sun in **AU** (sec. 2.4.1)
r_p	perihelion distance of Mercury (sec. 2.7.4)
S	solar constant (sec. 2.4.1)
T	surface temperature in °K (sec. 2.7.4)
T	atmospheric temperature in °K (table XIV, app. B)
T_A	atmospheric temperature at altitude z_A (app. B)
T_a	period of orbit about Mercury (sec. 2.2)
T_B	microwave brightness temperature (sec. 2.4.4, table I)
T_o	Mercury's orbital revolution period (sec. 2.1.3)
T_p	subsolar surface temperature at **perihelion** (sec. 2.7.4)
T_r	Mercury's rotation period (sec. 2.1.3)
U	ultraviolet **magnitude** (table XII)
u	mean atmospheric molecular weight (app. B)
V	visual **magnitude** (table XII)
V_e	escape velocity from Mercury (sec. 2.2)
V_s	solar wind speed (sec. 2.5.3)
y	penetration depth in cm (table XV)
Z	**zenith angle** of the Sun (sec. 2.7.4)
z	altitude above Mercury's surface (table XIV, app. B)
z_A	reference altitude in region of Mercury's atmosphere (app. B)
α	**phase angle** of Mercury (sec. 2.4.2)

a slope of portion of surface (fig. 9)

$\bar{a}$ mean slope (figs. 8 and 9)

β logarithmic atmospheric lapse rate (app. B)

Δ distance from reflecting surface to observer in AU (sec. 2.4.5) δ

δ ratio of electrical to thermal skin depths (tables IV and XVI)

ϵ dielectric constant (table IV)

θ angle from solar direction at Mercury (sec. 2.3)

λ wavelength of e-m radiation (sec. 2.4.2)

ρ density of surface material (table VI)

ρ density of atmosphere (table XIV, app. B)

$\overline{\rho}$ mean density of Mercury (sec. 2.1.2)

σ Stephan-Boltzmann constant, 5.67×10^{-5} erg°K^{-4} cm^{-2} sec^{-1} (sec. 2.4.3)

Φ solar wind **flux** (table XIII)

Φ_E cosmic ray **flux** for energy >E (sec. 2.5.1 and table XIII)

ϕ angle of dielectric **loss tangent** (tables IV and XVI)

$\phi(a)$ **phase function** (sec. 2.4.2)

Ψ gravitational potential (sec. 2.2)

Ω_M solid angle of sunlit surface of Mercury (sec. 2.4.2)

ω_r rotational angular velocity (sec. 2.1.3)

APPENDIX B
ATMOSPHERIC STRUCTURE RELATIONSHIPS

In terms of the symbols defined in appendix A, the model atmosphere in sections 2.6 and 3.6 is governed for each atmospheric region by

(1) hydrostatic equilibrium $$\frac{dP}{dz} = \rho g \tag{B1}$$

(2) the perfect gas law $$\rho = uP/R_g T \text{ , and} \tag{B2}$$

(3) a constant gradient $$\frac{d\, log\, T}{d\, log\, P} = \beta \tag{B3}$$

The solution of equations B1 through B3 requires that T and z at any value of P be related to those at T_A, z_A and P_A in the same region by

$$T = T_A\left(\frac{P}{P_A}\right)^{\beta} \tag{B4}$$

and

$$z = z_A - \frac{R_g}{\beta ug}(T - T_A) \tag{B5}$$

The lapse rate and scale heights are given by

$$dT/dz = \beta ug/R_g \tag{B6}$$

$$H_p = R_g T/ug \tag{B7}$$

and

$$H_\rho = H_p/(1-\beta). \tag{B8}$$

APPENDIX C
GLOSSARY*

Adhesion – Normal component of attractive molecular force-per-unit-area between unlike substances.

Angle of Internal Friction [ϕ] – If the ratio of tangential to normal external stress exceeds *tan* ϕ, slippage within the material occurs.

Anorthosite – **Igneous** rock, primarily **plagioclase**, on Earth crystallized at relatively high pressures below the surface.

Aphelion – That point in an orbit farthest from the Sun.

Astronomical Unit (AU) – The semi-major axis of the Earth's orbit about the Sun, approximately given by 1 AU = $1.49597893 \times 10^8 \pm 5$ km (ref. 6).

Basalt – Dark gray, **igneous** rock, primarily **plagioclase, pyroxene, ilmenite**, and magnetite, on Earth crystallized rapidly at relatively low pressures.

Cohesion – Normal component of attractive molecular force per unit area between like substances.

Color – For a given light source, the difference in **magnitude** for two bandwidths centered on different wavelengths.

Ecliptic – The plane which contains the mean orbit of the Earth about the Sun.

Flux – Rate of crossing an imaginary plane surface from one side to the other per unit time and per unit area for particles; for electromagnetic radiation, energy per unit wavelength or frequency interval, as well as per units time and area.

Geometric Albedo [$p(\lambda)$] – The ratio of the reflected **flux** (power per unit detector area) from an astronomical object (observed at distance Δ, zero **phase angle**, and zero optical depth) to the quotient of the solar power intercepted by the object divided by $\pi\Delta^2$, in the bandwidth considered. Here the **flux**, the power, and Δ must be expressed in consistent units; and Δ must be large compared to the dimensions of the object.

Heliocentric – Referenced to the center of the Sun.

Hermocentric – Referenced to the center of Mercury.

Igneous – Formed by solidification from a molten or partially molten state.

Ilmenite – A black mineral composed of an oxide of iron and titanium ($FeTiO_3$).

Integrated Flux – **Flux** of electromagnetic radiation integrated over all wavelengths or frequencies.

Intensity – **Flux** of electromagnetic radiation per unit solid angle of the source for a defining imaginary surface whose normal intersects the source; intensity is independent of the source-surface separation.

*Cross references within the glossary are indicated by bold face.

Loss Tangent (dielectric) – The ratio $2\sigma\lambda/\epsilon c$ (symbols defined in App. A); it is the capacity of a material to transmit a wave. Penetration depth increases with a decreasing value of the loss tangent.

Magnitude [m, m_o] – Five-halves times the common logarithm (base ten) of the ratio of the power received per unit area within some bandwidth for a standard object to that for an astronomical object. The base of this logarithmic scale is $x = 2.512$ so that an increase of one magnitude corresponds to a decrease in power by a factor x^{-1} or an increase in distance by a factor $x^{½}$. Apparent magnitudes (m) are those observed. Absolute magnitudes (m_o) are those for which absorption and scattering effects have been removed and observation is assumed to occur in a standard geometrical configuration. For solar system objects, the standard configuration is Sun-object distance $r = 1$ AU, object-observer distance $\Delta = 1$ AU, and **phase angle** $a = 0$.

Perihelion – That point in an orbit closest to the Sun.

Phase Angle [a] – The angle Sun-object-observer.

Phase Function [$\phi(a)$] – The ratio of the brightness at any **phase angle** a to the brightness at the **phase angle** ($a = 0$).

Phonon – The particle used in describing sound or vibration phenomena in matter, somewhat analogous to photon which can be defined as a particle used in describing electromagnetic radiation phenomena.

Plagioclase – Mineral of the feldspar family, composed of silicates of aluminum and sodium or calcium ($NaAlSi_3O_8$ or $CaAl_2Si_2O_8$).

Porosity – Ratio of the unoccupied volume to total volume.

Power Spectral Density – The Fourier transform of the autocorrelation function of the surface elevation.

Prograde – The direction of rotation and revolution common in the solar system in which the motion is counterclockwise as viewed from the north.

Pyroxene – A complex mineral composed of silicates of iron, magnesium, aluminum, and sodium or calcium.

Resonance – Orbital resonance occurs when the ratio of the orbital frequency to the rotational frequency equals the ratio of two integers. For Mercury this ratio is 2/3 and results in periodic repetition of a given geometric configuration (fig. 1).

Sidereal – Located with respect to the stars.

Thermal Conductivity [K] – Rate of heat energy transfer per unit time, area, and temperature gradient; specific to the material and depending on temperature if radiative energy transport is important.

Thermal Inertia – The quantity $(K\rho C)^{½}$ where $(K\rho C)$ is proportional to the natural unit of time for temperature variations within a material for contact **(phonon)** conduction.

Zenith Angle [Z] – Angular distance from the zenith at the observer's position. (The zenith is the direction above and perpendicular to the local horizon).

NASA SPACE VEHICLE DESIGN CRITERIA MONOGRAPHS

ENVIRONMENT

SP-8005	Solar Electromagnetic Radiation, revised May 1971
SP-8010	Models of Mars Atmosphere (1967), May 1968
SP-8011	Models of Venus Atmosphere (1968), December 1968
SP-8013	Meteoroid Environment Model–1969 (Near Earth to Lunar Surface), March 1969
SP-8017	Magnetic Fields–Earth and Extraterrestrial, March 1969
SP-8020	Mars Surface Models (1968), May 1969
SP-8021	Models of Earth's Atmosphere (120 to 1000 km), May 1969
SP-8023	Lunar Surface Models, May 1969
SP-8037	Assessment and Control of Spacecraft Magnetic Fields, September 1970
SP-8038	Meteoroid Environment Model–1970 (Interplanetary and Planetary), October 1970
SP-8049	The Earth's Ionosphere, March 1971
SP-8067	Earth Albedo and Emitted Radiation, July 1971
SP-8069	The Planet Jupiter (1970), December 1971
SP-8085	The Planet Mercury (1971), March 1972

STRUCTURES

SP-8001	Buffeting During Atmospheric Ascent, revised November 1970
SP-8002	Flight-Loads Measurements During Launch and Exit, December 1964
SP-8003	Flutter, Buzz, and Divergence, July 1964
SP-8004	Panel Flutter, July 1964
SP-8006	Local Steady Aerodynamic Loads During Launch and Exit, May 1965
SP-8007	Buckling of Thin-Walled Circular Cylinders, revised August 1968
SP-8008	Prelaunch Ground Wind Loads, November 1965
SP-8009	Propellant Slosh Loads, August 1968

SP-8012	Natural Vibration Modal Analysis, September 1968
SP-8014	Entry Thermal Protection, August 1968
SP-8019	Buckling of Thin-Walled Truncated Cones, September 1968
SP-8022	Staging Loads, February 1969
SP-8029	Aerodynamic and Rocket-Exhaust Heating During Launch and Ascent, May 1969
SP-8031	Slosh Suppression, May 1969
SP-8032	Buckling of Thin-Walled Doubly Curved Shells, August 1969
SP-8035	Wind Loads During Ascent, June 1970
SP-8040	Fracture Control of Metallic Pressure Vessels, May 1970
SP-8042	Meteoroid Damage Assessment, May 1970
SP-8043	Design–Development testing, May 1970
SP-8044	Qualification testing, May 1970
SP-8045	Acceptance testing, April 1970
SP-8046	Landing Impact Attenuation For Non-Surface-Planing Landers, April 1970
SP-8050	Structural Vibration Prediction, June 1970
SP-8053	Nuclear and Space Radiation Effects on Materials, June 1970
SP-8054	Space Radiation Protection, June 1970
SP-8055	Prevention of Coupled Structure-Propulsion Instability (Pogo), October 1970
SP-8056	Flight Separation Mechanisms, October 1970
SP-8057	Structural Design Criteria Applicable to a Space Shuttle, January 1971
SP-8060	Compartment Venting, November 1970
SP-8061	Interaction With Umbilicals and Launch Stand, August 1970
SP-8062	Entry Gasdynamic Heating, January 1971
SP-8063	Lubrication, Friction, and Wear, June 1971
SP-8066	Deployable Aerodynamic Deceleration Systems, June 1971
SP-8068	Buckling Strength of Structural Plates, June 1971
SP-8072	Acoustic Loads Generated by the Propulsion System, June 1971
SP-8077	Transportation and Handling Loads, September 1971

GUIDANCE AND CONTROL

SP-8015	Guidance and Navigation for Entry Vehicles, November 1968
SP-8016	Effects of Structural Flexibility on Spacecraft Control Systems, April 1969
SP-8018	Spacecraft Magnetic Torques, March 1969
SP-8024	Spacecraft Gravitational Torques, May 1969
SP-8026	Spacecraft Star Trackers, July 1970
SP-8027	Spacecraft Radiation Torques, October 1969
SP-8028	Entry Vehicle Control, November 1969
SP-8033	Spacecraft Earth Horizon Sensors, December 1969
SP-8034	Spacecraft Mass Expulsion Torques, December 1969
SP-8036	Effects of Structural Flexibility on Launch Vehicle Control Systems, February 1970
SP-8047	Spacecraft Sun Sensors, June 1970
SP-8058	Spacecraft Aerodynamic Torques, January 1971
SP-8059	Spacecraft Attitude Control During Thrusting Maneuvers, February 1971
SP-8065	Tubular Spacecraft Booms (Extendible, Reel Stored), February 1971
SP-8070	Spaceborne Digital Computer Systems, March 1971
SP-8071	Passive Gravity-Gradient Libration Dampers, February 1971
SP-8074	Spacecraft Solar Cell Arrays, May 1971
SP-8078	Spaceborne Electronic Imaging Systems, June 1971

CHEMICAL PROPULSION

SP-8025	Solid Rocket Motor Metal Cases, April 1970
SP-8041	Captive-Fired Testing of Solid Rocket Motors, March 1971
SP-8048	Liquid Rocket Engine Turbopump Bearings, March 1971
SP-8051	Solid Rocket Motor Igniters, March 1971
SP-8052	Liquid Rocket Engine Turbopump Inducers, May 1971

NASA-Langley, 1972 —— 30